Detection of PPM-UWB Random Signals

José A. López-Salcedo* and Gregori Vázquez

Signal Processing and Communications Group, Technical University of Catalonia (UPC)
c/ Jordi Girona 1-3, Mòdul D5-117, Campus Nord UPC, 08034 Barcelona, Spain
Email: {jlopez,gregori}@gps.tsc.upc.edu
Phone: +34 93 401 6454, Fax: +34 93 401 6447

EDICS: SPC-UWBC

Abstract

This paper focuses on the symbol detection problem of random PPM-UWB signals in the absence of inter-frame interference. Particular attention is devoted to severely time-varying channels where optimal detectors are proposed for both uncorrelated and correlated scattering scenarios. This is done by assuming the received waveforms to be unknown parameters. In UWB communication systems, the assumption of unknown random waveforms is consistent with the fact that the received waveform has very little resemblance with the original transmitted pulse. In order to circumvent this limitation, a conditional approach is presented herein by compressing the likelihood ratio test with the information regarding the second-order moments of the end-to-end channel response. Both full-rank and rank-one detectors are derived. For the reduced complexity rank-one detector, an iterative procedure is presented that maximizes the J-divergence between the hypotheses to be tested. Finally, simulation results are provided to compare the performance of the proposed detectors in different propagation environments.

I. Introduction

In the recent years ultra-wideband (UWB) communication systems have attracted the attention of many disciplines including, among others, antennas and propagation, electromagnetic compatibility, electronics

This work has been financed by the Spanish/Catalan Science and Technology Commissions and FEDER funds from the European Commission: TIC2003-05482 and 2005SGR-00639.

and signal processing for communications. Ultra-wideband technology is based on the emission of low-power and extremely-short pulses that occupy a very large bandwidth, and it is being considered for the next generation of wireless short-range communication systems [1]. Typically, UWB signals are defined to have an effective bandwidth larger than 500 MHz or a fractional bandwidth greater than 20%, according to the U.S. Federal Communications Commission (FCC) [2]. As a key feature, using such a very large bandwidth involves many intricate problems that do not appear in traditional narrowband communications.

One of the main problems with the transmission of UWB signals is that the received waveform has very little resemblance with the original transmitted pulse. There are several reasons for this to occur. First, the solid state pulse generating devices exhibit implementation imperfections such as random timing jitter or asymmetric polarity rising times that prevent the transmitted pulses to be all exactly the same [3]. Second, the radiating elements are found to differentiate the transmitted pulse [4], [5]. Third, the propagation environment is found to be terribly frequency-dependent and this causes a severe pulse distortion at the receiver [6]-[7]. Fourth, experimental results show that pulse distortion is also path-dependent and thus, different pulse distortions are experienced when propagating through different paths [8]. As a result of these impairments, but especially when the propagation paths change due to the relative movement between transmitter and receiver, the end-to-end channel response can be assumed to be time-varying. In some applications, however, the paths can also change as a result of moving scatterers caused by moving persons in indoor scenarios [9]. In these circumstances it is reasonable to assume that the received waveforms are all random. This will be the starting hypothesis for the study to be presented herein.

It is interesting to remark that in those UWB applications where the channel remains static for a long time, traditional signal processing techniques for narrowband communication systems can still be applied. When channel information is available, this involves a *deterministic* approach based on applying the well-known matched-filter principle to all the propagation paths (see, for instance, [10], [11], [12] or [13] among many other). When no channel state information is available but some feedback between receiver and transmitter is allowed, a promising approach is to use time-reversal as indicated in [14], [15]. However, a rather different approach must be adopted when the channel becomes severely time-varying. In that case it is reasonable to assume that the received signal is *random*. Consequently, the symbol decision strategy cannot rely on the specific shape of the received waveform but on the underlying statistics of the received signal. Clearly this is a problem of non-coherent signal detection, a topic that has received significant attention in the last decades with many important contributions to RADAR and SONAR applications [16], [17], among many other.

Due to the absence of channel state information and the adoption of non-coherent detection, multi-level signaling based on pulse-amplitude modulation (PAM) cannot be adopted. For this reason the work to be presented herein is based on pulse-position modulation (PPM). For the sake of simplicity, this paper will focus on the non-coherent symbol detection problem of *binary*-PPM UWB signals. Based on the statistical characterization of the received waveform, the symbol detection problem is formulated within the framework of likelihood ratio testing for the low-SNR regime. On the one hand, the low-SNR assumption can be understood as a realistic hypothesis to the real working conditions of UWB systems. On the other hand, operating under the low-SNR regime allows the analytical tractability of the detection problem and the applicability of maximum likelihood techniques as in [18]. Once the optimal symbol decision statistics are derived, different practical cases of interest are further analyzed. For instance, an information-theoretic based receiver is proposed as a tradeoff between performance and implementation complexity in the presence of correlated scattering. The result is a gradient based scheme that provides the best and the simplest receiver filter for maximizing the divergence measure of the symbol decision problem. Simulation results are presented to evaluate the performance of the proposed receivers and insightful links are established with existing contributions in the recent literature.

The paper is organized as follows. The signal model and problem statement are introduced in Section II. The estimation of the actual propagation statistics is presented in Section III. Next, the optimal low-SNR symbol decision rule is provided in Section IV. The particularization of this symbol decision strategy to the case of uncorrelated and correlated scattering is analyzed in Section V and Section VI, respectively. Finally, simulation results are discussed in Section VII and conclusions are drawn in Section VIII.

II. Signal Model and Problem Statement

A. Modulation format

The signal model to be considered in this paper assumes the transmission of ultra-short pulses with binary pulse-position modulation (2-PPM). The transmission of every single information bearing symbol is implemented by the repetition of N_f low-power pulses. Each of these pulses is confined within a frame duration of N_{sf} samples that must be sufficiently large so as to avoid interframe interference between consecutive frames. Consequently, the frame duration must encompass the maximum delay spread of the channel and the maximum time-shift introduced by the PPM modulation and the time-hopping (TH) sequence. Since we focus on the symbol decision problem, the TH sequence is assumed to have been previously acquired in a prior stage of the receiver. Thus, no TH is assumed hereafter.

At the receiver, the transmitted pulses arrive in the form of distorted waveforms. This degradation is caused by the inherent distortion produced by the wideband radiating elements, but especially, because of the propagation physics of UWB signals. In this sense, and similar to [19], an *unstructured* approach is adopted for modeling the received signal. That is, we completely disregard the paths of the propagation channel and we just consider the received waveform as a whole. This received waveform is denoted by the discrete-time representation $g(k)$ and the whole received signal can be expressed as,

$$r(k) = \sum_{n=-\infty}^{\infty} c_n \sum_{i=0}^{N_f-1} g_{n,i}\left(k - d_n N_\Delta - iN_{sf} - nN_{ss}\right) + n(k) \tag{1}$$

with N_Δ the number of samples for the PPM time-shift, N_{sf} the number of samples per frame (i.e. the frame duration) and N_{ss} the number of samples per symbol (i.e. the symbol duration). Because of the frame repetition within the symbol duration, the number of samples per symbol is $N_{ss} = N_f N_{sf}$. Since binary PPM is adopted, the pulse-position symbols are restricted to $d_n = \{0, 1\}$. Moreover, the sequence $c_n = \{-1, 1\}$ accounts for the polarity randomization code that is introduced in order to avoid the existence of spectral lines that may violate spectral regulations [20]. Finally, $n(k)$ incorporates the contribution of both the thermal noise and the interference signal. That is, $n(k) = w(k) + i(k)$ where $w(k)$ are the zero-mean Gaussian samples of thermal noise with variance σ_w^2 and $i(k)$ is the interference signal to be described in Section II-B.

Regarding the received waveform, note that $g_{n,i}(k)$ in (1) stands for the received waveform corresponding to the n-th symbol and the i-th frame. The received waveforms $g_{n,i}(k)$ have a finite time support of N_g samples and the indexation $\{n, i\}$ is consistent with the fact that the received waveform may possibly differ from frame to frame. For instance, this variation in the received waveforms may be caused by the relative movement between transmitter and receiver but also because of moving scatterers like moving persons [9]. Moreover, and similarly to spread-spectrum systems, the timing error can be decomposed into frame-level (i.e. *coarse*) timing error and pulse-level (i.e. *fine*) timing error. The signal model in (1) assumes that the frame-level timing error has been previously acquired so that the residual pulse-level timing error becomes part of the shape of the unknown waveform [18].

With the above considerations, let us express the signal model in (1) into a more compact matrix notation. To this end let us divide the observation interval into a total of L segments $\mathbf{r}_n$, each with a length equal to the symbol duration N_{ss}. By doing so, the observation interval assumes the transmission of L binary-PPM symbols. Similarly, let us divide each received symbol vector $\mathbf{r}_n$ into a total of N_f segments $\mathbf{r}_{n,i}$ with dimensions $(N_{sf} \times 1)$ corresponding to the N_f frames within a symbol duration. That is, $\mathbf{r}_n = \left[\mathbf{r}_{n,0}^T, \mathbf{r}_{n,1}^T, \ldots, \mathbf{r}_{n,N_f-1}^T\right]^T$. According to the structure of binary PPM, the received signal for

each frame interval can be expressed as follows,

$$\mathbf{r}_{n,i} = \begin{cases} c_n \mathbf{\Pi} \mathbf{g}_{n,i} + \mathbf{n}_{n,i} & : \quad d_n = 1 \\ c_n \mathbf{J}_{N_\Delta} \mathbf{\Pi} \mathbf{g}_{n,i} + \mathbf{n}_{n,i} & : \quad d_n = 0 \ . \end{cases} \tag{2}$$

Matrices $\mathbf{\Pi}$ and $\mathbf{J}_{N_\Delta}$ in (2) are a $(N_{sf} \times N_g)$ zero-padding matrix and a $(N_{sf} \times N_{sf})$ N_Δ-samples time-shift matrix, respectively. That is, $\mathbf{\Pi} \doteq [\mathbf{I}_{(N_g \times N_g)} \mathbf{0}_{(N_g \times N_{sf} - N_g)}]^T$ whereas $[\mathbf{J}_{N_\Delta}]_{i,j} = 1$ for $(j-i) = N_\Delta$ and $[\mathbf{J}_{N_\Delta}]_{i,j} = 0$ for $(j-i) \neq N_\Delta$. Finally, the $(N_g \times 1)$ vector $\mathbf{g}_{n,i}$ incorporates the N_g samples of the received waveform for the n-th symbol and i-th frame, and $\mathbf{n}_{n,i}$ the corresponding samples of the noise and interference contribution.

B. Interference signal model

The two main features of UWB communication systems are their very large spectral occupancy and their very low power spectral density. The spectral occupancy of UWB signals is on the order of a few GHz and this forces UWB signals to coexist with most of the existing wireless communication systems. However, the very large spectral occupancy of UWB signals makes current wireless communication systems to be perceived as narrowband interferences by a UWB receiver. In particular, the most significant source of interference are IEEE 802.11a WLAN devices, whose central frequency is located around 5 GHz with a transmitted bandwidth on the order of 20 MHz. These narrowband interference sources can be considered to be high-power sources compared to UWB signals [21].

The Gaussian signal model is assumed in this paper for modeling the interference signals arriving at an UWB receiver. As in [11] or [22], the interference signals are assumed to be discrete-time pass-band Gaussian random processes with zero-mean and spectral density $S_{\mathrm{I}}(f)$ characterized by a central frequency f_{I} and a bandwidth occupancy $\mathrm{BW_I}$ as follows,

$$S_{\mathrm{I}}(f) = \begin{cases} \frac{N_{\mathrm{I}}}{2}, & f_{\mathrm{I}} - \frac{\mathrm{BW_I}}{2} \geq |f_I| \geq f_{\mathrm{I}} + \frac{\mathrm{BW_I}}{2} \\ 0, & \text{otherwise.} \end{cases} \tag{3}$$

Consequently the interference $i(k)$ for the equivalent noise term $n(k) = w(k) + i(k)$ in (1) is characterized by a covariance matrix $\mathbf{C}_{\mathrm{I}}$ whose (i,j) entries are given by $[\mathbf{C}_{\mathrm{I}}]_{i,j} = P_{\mathrm{I}} \cdot sinc\left(\mathrm{BW_I}\,(i-j)\right) cos\left(2\pi f_{\mathrm{I}}\,(i-j)\right)$ with $P_{\mathrm{I}} = N_{\mathrm{I}} \cdot \mathrm{BW_I}$ the interference power.

C. UWB channel model and operating conditions

Certainly, the optimal design of a communication system must take into consideration the propagation conditions of the transmitted signal on its way to the receiver end. However many issues related with the

propagation conditions of UWB signals are still under study. This is due to the fact that, although UWB technology has been around since the 60s, most channel measurement campaigns are being performed in the recent years. Therefore, there is still a lot to be learned about the propagation characteristics of UWB signals and more measurement campaigns are still required [23].

The most common characteristic of UWB transmissions is the extremely frequency-dependent and path-dependent transfer function. From a stochastic point of view, some authors indicate that the statistical modeling of the measured small-scale fading is related to the Nakagami distribution [24], or to the lognormal distribution [25]. These results for high data rate UWB systems in residential and office environments were included in the IEEE 802.15.3a channel model [25]. However, UWB channels measured by other authors were found to be not so different from traditional channels. For instance, measurement campaigns were carried out with both moving and fixed terminals in open space environments such as a lobby [9], [26], and in industrial environments [27]. For these propagation environments, the small-scale fading statistics of the received waveforms were found to be closer to the traditional Rayleigh and Rice distributions rather than to Nakagami and lognormal distributions assumed in IEEE 802.15.3a channel models. Similarly to traditional wideband channels, the Rayleigh distribution was found to comply with moving terminals whereas the Rice distribution was found to comply with static terminals. This is somehow surprising because the very large bandwidth of UWB signals is often argued for not assuming the traditional Gaussian distribution for the channel tap amplitudes. These new results for low data-rate applications in industrial, outdoor or rural environments were included in the IEEE 802.15.4 channel models [28].

In the present paper, the Gaussian approach suggested by [9], [26] or [27] is adopted for mathematical tractability. Consequently, the samples of the received waveforms are modeled by a zero-mean random Gaussian process driven by a $(N_g \times N_g)$ covariance matrix $\mathbf{C}_g$. According to the signal model in Section II, let us indicate the hypothesis of transmitting $d_n = 1$ by $\mathcal{H}_+$ and the hypothesis of transmitting $d_n = 0$ by $\mathcal{H}_-$. Under hypothesis $\mathcal{H}_+$, the conditional probability density function for the n-th received symbol is given by the multivariate Gaussian probability density function as follows,

$$p\left(\mathbf{r}_n|\mathcal{H}_+, \mathbf{C_g}\right) = \prod_{i=0}^{N_f-1} \frac{1}{(2\pi)^{N_{sf}/2} \det^{1/2}\left(\mathbf{C}_+ + \mathbf{C}_{\mathrm{N}}\right)} \exp\left(-\frac{1}{2}\mathbf{r}_{n,i}^T \left(\mathbf{C}_+ + \mathbf{C}_{\mathrm{N}}\right)^{-1} \mathbf{r}_{n,i}\right) \quad (4)$$

with $\mathbf{C}_+ \doteq \mathbf{\Pi C_g \Pi}^T$ the covariance matrix for the signal received under $\mathcal{H}_+$ and $\mathbf{C}_{\mathrm{N}} \doteq \sigma_w^2\mathbf{I} + \mathbf{C}_{\mathrm{I}}$ the covariance matrix for the Gaussian contribution of both thermal noise and interference. Similarly, the probability density function under hypothesis $\mathcal{H}_-$ is found by substituting $\mathbf{C}_+$ with $\mathbf{C}_-$ in (4).

It is important to note that the probability density function in (4) is conditioned on the covariance matrix

$\mathbf{C_g}$. This covariance matrix $\mathbf{C_g}$ is unknown since it conveys the information regarding the second-order statistics of the actual received waveforms, which are usually unknown and depend on the particular transmission/reception set-up and propagation conditions. Therefore the covariance matrix $\mathbf{C_g}$ can be regarded as a nuisance parameter that has to be estimated. Replacing $\mathbf{C_g}$ with a suitable estimate leads to a compressed or conditional approach where the symbol decision statistics do not depend on $\mathbf{C_g}$ anymore. This conditional approach is presented in Section V and Section VI, whereas the estimate for $\mathbf{C_g}$ is to be presented next in Section III.

III. Estimation of the Unknown Channel Covariance Matrix

Because of the unknown distortion suffered by the transmitted pulse, the covariance matrix $\mathbf{C_g}$ of the Gaussian random received waveform model is also unknown. However this covariance matrix is ultimately required for evaluating the symbol decision statistics and thus, it must be estimated from the incoming data. To do so, an estimate for $\mathbf{C_g}$ is presented herein based on the least-squares principle. The key point is to exploit the structure of the frame-level synchronous autocorrelation matrix of the received data. Let us denote the $(N_{sf} \times N_{sf})$ frame-level synchronous autocorrelation matrix by $\mathbf{R}$. Then the signal model for $\mathbf{R}$ is given by

$$\mathbf{R} = \frac{1}{2}\left[\mathbf{C}_+ + \mathbf{C}_-\right] + \mathbf{C}_{\mathrm{N}}. \tag{5}$$

The signal model in (5) assumes binary-PPM with equiprobable symbols. In this sense, the observation interval must be large enough so as to guarantee the equiprobability of received symbols (e.g. $L > 100$). Since $\mathbf{C}_+ \doteq \mathbf{\Pi C_g \Pi}^T$ and $\mathbf{C}_- \doteq \mathbf{J}_{N_\Delta}\mathbf{\Pi C_g \Pi}^T\mathbf{J}_{N_\Delta}^T$ according to Section II-A, the following least-squares criterion can be formulated

$$\widehat{\mathbf{C}}_{\mathbf{g}} = \arg\min_{\mathbf{C_g}} \left\| \widehat{\mathbf{R}} - \frac{1}{2}\left[\mathbf{\Pi C_g \Pi}^T + \mathbf{J}_{N_\Delta}\mathbf{\Pi C_g \Pi}^T\mathbf{J}_{N_\Delta}^T\right] - \mathbf{C}_{\mathrm{N}} \right\|_F^2. \tag{6}$$

In (6), $\widehat{\mathbf{R}}$ stands for the estimate of the synchronous autocorrelation matrix,

$$\widehat{\mathbf{R}} = \frac{1}{LN_f}\sum_{n=0}^{L-1}\sum_{i=0}^{N_f-1}\mathbf{r}_{n,i}\mathbf{r}_{n,i}^T = \frac{1}{L}\sum_{n=0}^{L-1}\widehat{\mathbf{R}}_n \tag{7}$$

With the above considerations, and since $\|\mathbf{A}\|_F^2 = Tr\left(\mathbf{A}^T\mathbf{A}\right) = vec^T\left(\mathbf{A}\right)vec\left(\mathbf{A}\right)$ for any real matrix $\mathbf{A}$, the unique solution to the least-squares problem in (6) is given by,

$$\widehat{\mathbf{C}}_{\mathbf{g}} \;=\; \mathbf{\Pi}^T vec^{-1}\left(\left(\mathbf{A}_{\mathrm{S}}^T\mathbf{A}_{\mathrm{S}}\right)^{-1}\mathbf{A}_{\mathrm{S}}^T vec\left(\widehat{\mathbf{R}} - \mathbf{C}_{\mathrm{N}}\right)\right)\mathbf{\Pi} \tag{8}$$

with $\mathbf{A}_{\mathrm{S}} \doteq \mathbf{I} + \mathbf{J}_{N_\Delta} \otimes \mathbf{J}_{N_\Delta}$ the so-called *mixture* matrix, representing the linear mapping of the covariance matrix $\mathbf{C_g}$ onto the synchronous autocorrelation of the received data. In addition, $vec^{-1}(\cdot)$ stands for the

inverse of the column-stacking $vec(\cdot)$ operator [1]. Finally note that the mixture matrix $\mathbf{A}_{\mathrm{S}}$ is a constant matrix that can be calculated offline. This is because the matrix $\mathbf{A}_{\mathrm{S}}$ only depends on the time-shift N_{Δ} which is usually a-priori known at the receiver.

IV. Optimal Symbol Decision Statistics

This paper proposes a fully stochastic approach for addressing the symbol detection problem of random UWB signals. By doing so, the time-varying behavior of the unknown propagation conditions can be easily incorporated into the model. Next, the optimal test statistics for the binary-PPM decision problem are presented and the relationship with some previous contributions in the literature is overviewed.

A. Log-GLRT for the binary-PPM decision problem

Since the received waveforms are assumed to be random, the symbol detection problem must rely on the statistical properties of the received data rather than on the particular shape of the received waveforms. The optimal symbol decision statistics will be derived based on the generalized likelihood ratio test (GLRT) which maximizes the probability of detection for a given probability of false alarm [17]. The GLRT just requires the knowledge of the probability density function for the hypotheses to be tested. For the problem at hand, two hypotheses must be decided depending on whether $d_n = 1$ or $d_n = 0$. Thus, the GLRT is obtained by evaluating the ratio

$$\Lambda(\mathbf{r}_n|\mathbf{C}_{\mathbf{g}}) \doteq \frac{p\left(\mathbf{r}_n|\mathcal{H}_+, \mathbf{C}_{\mathbf{g}}\right)}{p\left(\mathbf{r}_n|\mathcal{H}_-, \mathbf{C}_{\mathbf{g}}\right)} \tag{9}$$

and deciding $d_n = 1$ when $\Lambda(\mathbf{r}_n|\mathbf{C}_{\mathbf{g}}) > 1$ or $d_n = 0$ when $\Lambda(\mathbf{r}_n|\mathbf{C}_{\mathbf{g}}) < 1$.

At this point, two important assumptions are considered. First, the noise and the interference signals are considered high-power sources compared to the UWB signal. Second, the very large bandwidth of UWB signals allows us to assume that interference signals from existing wireless services are all narrowband. This second assumption is reasonable because the bandwidth of UWB signals is on the order of a few GHz whereas the bandwidth of existing wideband wireless systems is on the order of 10 to 20 MHz (e.g. IEEE802.11a/b/g wireless LAN devices).

With the above considerations, the logarithm can be applied to both sides of (9). Then a simple expression is obtained for the log-GLRT decision rule for binary-PPM,

$$L'(\mathbf{r}_n|\mathbf{C}_{\mathbf{g}}) = Tr\left(\left[\mathbf{C}_+ - \mathbf{C}_-\right]\widehat{\mathbf{R}}_n\right) \tag{10}$$

[1]The solution can also be formulated in terms of the $vech(\cdot)$ operator which eliminates the redundancy of symmetric matrices by just considering the entries on and below the main diagonal.

where $\{\mathbf{C}_+, \mathbf{C}_-\}$ are the frame-level covariance matrices for the signal model under hypotheses $\{\mathcal{H}_+, \mathcal{H}_-\}$, and $\widehat{\mathbf{R}}_n$ is the estimate of the frame-level synchronous autocorrelation matrix during the n-th received symbol duration. That is,

$$\widehat{\mathbf{R}}_n \doteq \frac{1}{N_f} \sum_{i=0}^{N_f-1} \mathbf{r}_{n,i}\mathbf{r}_{n,i}^T. \tag{11}$$

All the analytic derivations to obtain (10) are omitted for clarity reasons but they are all given in Appendix A and Appendix B. Finally, the symbol decision rule can be implemented as $\widehat{d}_n \doteq \frac{1}{2}\left[1 + sign\left\{L'(\mathbf{r}_n|\mathbf{C_g})\right\}\right]$.

Note that $\mathbf{C}_+$ and $\mathbf{C}_-$ in (10) depend on $\mathbf{C_g}$ according to Section II-A. Since the covariance matrix $\mathbf{C_g}$ is unknown, it must be first estimated from the incoming data. An estimate for $\mathbf{C_g}$ was already presented in (8) and the compression of the log-GLRT with this estimate will be presented later on in Section V and Section VI. Finally, note that for the particular case of a constant waveform, both $\mathbf{C}_+$ and $\mathbf{C}_-$ would be rank-one matrices and the detector in (10) would naturally lead to the matched filter detector.

B. Relationship of the proposed log-GLRT with existing literature

The log-GLRT presented in (10) is a rather general result for the symbol detection problem of binary-PPM UWB signals under the assumptions of low signal-to-noise ratio and low signal-to-interference ratio. In this sense, it is interesting to note that many of the receivers heuristically proposed in the existing literature are indeed particular cases of the more general result in (10).

For instance, the log-GLRT can be understood as a balanced second-order matched filter. Let us denote the difference matrix $\mathbf{C}_+ - \mathbf{C}_-$ in (10) by $\mathbf{P}$, that is, $\mathbf{P} \doteq \mathbf{C}_+ - \mathbf{C}_-$. Thus, $\mathbf{P}$ becomes the correlation template for deciding between the hypotheses $\mathcal{H}_+$ and $\mathcal{H}_-$, similarly to what occurs for the binary symbol detection problem with deterministic signals. In that case, the correlation template has impulse response $p(k) = g(k) - g(k - N_\Delta)$ [29] which is indeed the scalar version of the second-order template $\mathbf{P}$.

Another important point to be highlighted is that no matrices are required to be inverted in the test statistics in (10). This is in contrast with traditional detectors for random signals, where the inverse of covariance matrices is usually required [16]. The key point here is that the result in (10) is derived for the low-SNR regime, where the main degradation is caused by the thermal noise. As a result the optimal test statistics are found to rely on the signal subspace of the received data rather than on the noise subspace. Therefore a more robust performance is expected in front of the noise at the expense of a limiting floor effect for the high signal-to-noise scenarios. This floor effect phenomenon is explained as the degradation

resulting from the noise introduced by the algorithm itself [30] and it is commonly exhibited by most low-SNR techniques.

Apart from the above considerations, the result in (10) includes the energy-detector receiver [31], [32]. This is a suboptimal receiver that can be obtained from (10) by forcing uncorrelated scattering with a constant power delay profile. The eigen-based received in [33] can also be obtained from (10) and it aims at finding the best deterministic template for the linear filtering of random received data. Finally, (10) under the assumption of uncorrelated scattering results in the receiver proposed in [34].

V. Optimal Receiver under the Uncorrelated Scattering Assumption

In the presence of uncorrelated scattering (US) the covariance matrix of the received waveform becomes diagonal. That is,

$$\mathbf{C_g} = diag\left(\boldsymbol{\gamma}\right) \tag{12}$$

with $\boldsymbol{\gamma} = [\gamma(0), \gamma(1), \ldots, \gamma(N_g - 1)]^T$ the power-delay profile (PDP) of the end-to-end channel response (i.e. the PDP of the received waveforms). Consequently the frame-level covariance matrices for the hypotheses $\{\mathcal{H}_+, \mathcal{H}_-\}$ become $\mathbf{C}_+ = diag\left(\tilde{\boldsymbol{\gamma}}\right)$ and $\mathbf{C}_- = diag\left(\mathbf{J}_{N_\Delta}\tilde{\boldsymbol{\gamma}}\right)$, respectively. Note that $\tilde{\boldsymbol{\gamma}} \doteq \boldsymbol{\Pi}\boldsymbol{\gamma}$ is the $(N_{sf} \times 1)$ zero-padded version of the $(N_g \times 1)$ PDP indicated by $\boldsymbol{\gamma}$ in (12).

In the sequel, the log-GLRT will be particularized first for the case of a-priori known PDP. This will provide insightful relationships with existing contributions in the literature. Second, the conditional log-GLRT will be presented which considers the nuisance PDP as a deterministic parameter to be estimated.

A. Log-GLRT under the assumption of known power-delay profile

Let us assume the PDP to be known at the receiver. Then, the conditioned log-GLRT results in

$$L'(\mathbf{r}_n|\tilde{\boldsymbol{\gamma}}) = Tr\left(diag\left(\tilde{\boldsymbol{\gamma}} - \mathbf{J}_{N_\Delta}\tilde{\boldsymbol{\gamma}}\right)\widehat{\mathbf{R}}_n\right) = Tr\left(diag(\mathbf{w})\widehat{\mathbf{R}}_n\right) \tag{13}$$

$$= \sum_{k=0}^{N_{sf}-1} w(k) \sum_{i=0}^{N_f-1} r_{n,i}^2(k) \tag{14}$$

where the optimal correlation template $\mathbf{w}$ is defined as $\mathbf{w} \doteq \tilde{\boldsymbol{\gamma}} - \mathbf{J}_{N_\Delta}\tilde{\boldsymbol{\gamma}}$. The receiver implementation for the test statistics in (14) is shown in Fig. 1.

The structure in (14) is similar to that of the MLRP receiver in [34] where the received waveform was modeled as a continuous-time filtered Gaussian process. However, the weighting function $w(k)$ for the MLRP receiver depends on the inverse of the noise power and thus, it significantly degrades in the

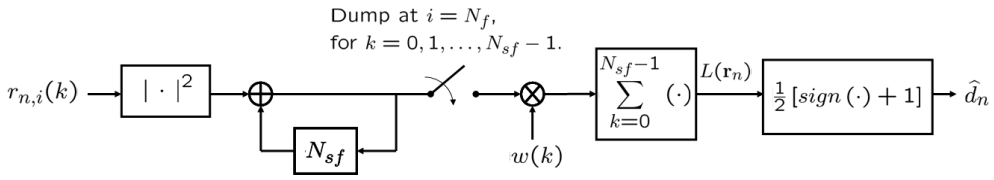

Fig. 1. Optimal detector for random binary-PPM signals with uncorrelated scattering when the PDP is a priori known.

low-SNR regime. On the contrary, the weighting function $w(k)$ in (14) does not depend on the noise power but just on the power-delay profile and thus, a more robust performance is expected.

It is also interesting to point out that the PDP-receiver proposed in (14) particularizes to the well-known energy-detector receiver [31] when the power-delay profile is constant. In that case, $\boldsymbol{\gamma} = \gamma \mathbf{1}_{N_g}$ for some positive constant γ and $\mathbf{1}_n$ an all ones $(n \times 1)$ vector[2]. Then the weighting function $w(k)$ becomes the difference of two noncoherent integrations of received samples.

B. Conditional log-GLRT

When the power-delay profile $\boldsymbol{\gamma}$ is not a priori known, a possible approach is to consider it as an unknown deterministic nuisance parameter that has to be estimated. An estimate for the zero-padded power-delay profile $\tilde{\boldsymbol{\gamma}}$ is proposed here based on the least-squares cost function introduced in (8). For the case of uncorrelated scattering the cost function in (8) simplifies to[3]

$$\widehat{\tilde{\boldsymbol{\gamma}}} = \arg\min_{\tilde{\boldsymbol{\gamma}}} \left\| diag(\mathbf{R}) - \frac{1}{2}\left(\mathbf{I} + \mathbf{J}_{N_\Delta}\right)\tilde{\boldsymbol{\gamma}} - \left(\sigma_w^2 + P_{\mathrm{I}}\right)\mathbf{1} \right\|^2. \tag{15}$$

Therefore, the least-squares estimate for the zero-padded power-delay profile $\tilde{\boldsymbol{\gamma}}$ is given by

$$\widehat{\tilde{\boldsymbol{\gamma}}} = \left(\mathbf{B}_{\mathrm{S}}^T \mathbf{B}_{\mathrm{S}}\right)^{-1} \mathbf{B}_{\mathrm{S}}^T diag\left(\mathbf{R} - \left(\sigma_w^2 + P_{\mathrm{I}}\right)\mathbf{I}\right) \tag{16}$$

with $\mathbf{B}_{\mathrm{S}} \doteq \mathbf{I} + \mathbf{J}_{N_\Delta}$ the *mixture* matrix representing the linear mapping of the power-delay profile onto the synchronous autocorrelation of the received data. Plugging (16) into the log-GLRT in (10), and taking into consideration the diagonal structure of $\widehat{\mathbf{R}}_n$ under the US assumption,

$$\begin{aligned} L'(\mathbf{r}_n) &= \left(\widehat{\tilde{\boldsymbol{\gamma}}} - \mathbf{J}_{N_\Delta}\widehat{\tilde{\boldsymbol{\gamma}}}\right)^T diag\left(\widehat{\mathbf{R}}_n\right) = \widehat{\tilde{\boldsymbol{\gamma}}}^T \left(\mathbf{I} - \mathbf{J}_{N_\Delta}\right)^T diag\left(\widehat{\mathbf{R}}_n\right) && (17) \\ &= diag^T\left(\mathbf{R} - \left(\sigma_w^2 + P_{\mathrm{I}}\right)\mathbf{I}\right)\mathbf{B}_{\mathrm{S}}\left(\mathbf{B}_{\mathrm{S}}^T\mathbf{B}_{\mathrm{S}}\right)^{-1}\mathbf{B}_{\mathrm{D}}^T diag\left(\widehat{\mathbf{R}}_n\right) && (18) \end{aligned}$$

[2]When omitted, the dimensions of the all ones vector $\mathbf{1}$ and the identity matrix $\mathbf{I}$ are $(N_{sf} \times 1)$ and $(N_{sf} \times N_{sf})$, respectively.

[3]The $diag(\cdot)$ operator returns the main diagonal when the argument is a matrix and it returns a diagonal matrix when the argument is a vector.

with $\mathbf{B}_{\mathrm{D}} \doteq \mathbf{I} - \mathbf{J}_{N_\Delta}$ the *separation* matrix representing the linear mapping of the power-delay profile onto the weighting function $\mathbf{w}$ in (13). Since the mixture matrix $\mathbf{B}_{\mathrm{S}}$ is full rank, then $\left(\mathbf{B}_{\mathrm{S}}^T\mathbf{B}_{\mathrm{S}}\right)^{-1} = \mathbf{B}_{\mathrm{S}}^{-1}\left(\mathbf{B}_{\mathrm{S}}^T\right)^{-1}$ and the log-GLRT in (18) can be recast as

$$L'(\mathbf{r}_n) = diag^T\left(\mathbf{R} - \left(\sigma_w^2 + P_{\mathrm{I}}\right)\mathbf{I}\right)\left(\mathbf{B}_{\mathrm{S}}^T\right)^{-1}\mathbf{B}_{\mathrm{D}}^T diag\left(\widehat{\mathbf{R}}_n\right). \tag{19}$$

Note that the log-GLRT in (19) can be understood as a two-step procedure. First, the binary-PPM mixed data is separated from the synchronous autocorrelation matrix $\mathbf{R}$ by using the inverse of the mixture matrix $\mathbf{B}_{\mathrm{S}}$. Second, the hypothesis testing template is built with the separation matrix $\mathbf{B}_{\mathrm{D}}$ and the result is correlated with the data from the n-th symbol synchronous autocorrelation matrix $\widehat{\mathbf{R}}_n$. Note that both $\mathbf{B}_{\mathrm{S}}$ and $\mathbf{B}_{\mathrm{D}}$ are a-priori known at the receiver since they only depend on the time-shift N_Δ. Thus, the matrix product $\left(\mathbf{B}_{\mathrm{S}}^T\right)^{-1}\mathbf{B}_{\mathrm{D}}^T$ in (19) can be calculated offline.

VI. Optimal Receiver under the Correlated Scattering Assumption

In the presence of correlated scattering (CS), the only assumption to be made is that the covariance matrix $\mathbf{C_g}$ is symmetric positive semidefinite with decreasing entries along diagonals[4]. In the sequel, the conditional decision statistics for the CS assumption are provided first based on the compression of the log-GLRT with the full-rank estimation of $\mathbf{C_g}$. Later on, a simplification is presented based on selecting a single eigenmode of $\mathbf{C_g}$ so as to implement a low-complexity rank-one detector.

A. Conditional log-GLRT

In order to evaluate the symbol decision rule, the log-GLRT in (10) must be first compressed with the information regarding the unknown channel response. To this end, let us first express the log-GLRT explicitly as a function of $\mathbf{C_g}$. Using the signal model in Section II we have that

$$\begin{aligned} L'\left(\mathbf{r}_n|\mathbf{C_g}\right) &= Tr\left(\left[\mathbf{\Pi}\mathbf{C_g}\mathbf{\Pi}^T - \mathbf{J}_{N_\Delta}\mathbf{\Pi}\mathbf{C_g}\mathbf{\Pi}^T\mathbf{J}_{N_\Delta}^T\right]\widehat{\mathbf{R}}_n\right) &(20)\\ &= vec^T\left(\mathbf{\Pi}\mathbf{C_g}\mathbf{\Pi}^T\right)\mathbf{A}_{\mathrm{D}}^T vec\,\widehat{\mathbf{R}}_n. &(21)\end{aligned}$$

In (21), we have used the properties $Tr\left(\mathbf{A}^T\mathbf{B}\right) = vec^T\left(\mathbf{A}\right)vec\left(\mathbf{B}\right)$ and $vec\left(\mathbf{ABC}\right) = \left(\mathbf{C}^T\otimes\mathbf{A}\right)vec\left(\mathbf{B}\right)$ for any $\mathbf{A}$, $\mathbf{B}$ and $\mathbf{C}$ matrices for which the product $\mathbf{A}^T\mathbf{B}$ and $\mathbf{ABC}$ is defined.

Similarly to the US case, the *separation* matrix $\mathbf{A}_{\mathrm{D}}$ in (21) is defined as $\mathbf{A}_{\mathrm{D}} \doteq \mathbf{I} - \mathbf{J}_{N_\Delta}\otimes\mathbf{J}_{N_\Delta}$. Substituting the covariance matrix $\mathbf{C_g}$ with the estimate $\widehat{\mathbf{C}}_g$ in Section III, the log-GLRT results in

$$L'\left(\mathbf{r}_n\right) = vec^T\left(\widehat{\mathbf{R}} - \mathbf{C}_{\mathrm{N}}\right)\mathbf{A}_{\mathrm{S}}\left(\mathbf{A}_{\mathrm{S}}^T\mathbf{A}_{\mathrm{S}}\right)^{-1}\mathbf{A}_{\mathrm{D}}^T vec\,\widehat{\mathbf{R}}_n. \tag{22}$$

[4]Toeplitz structure does not apply to this covariance matrix since the path-loss results in non-WSS random Gaussian waveforms.

Since the mixture matrix $\mathbf{A}_{\mathrm{S}}$ is a full-rank matrix, then $\left(\mathbf{A}_{\mathrm{S}}^{T}\mathbf{A}_{\mathrm{S}}\right)^{-1} = \mathbf{A}_{\mathrm{S}}^{-1}\left(\mathbf{A}_{\mathrm{S}}^{T}\right)^{-1}$ and the log-GLRT in (22) can be equivalently expressed as

$$L'\left(\mathbf{r}_n\right) \;=\; vec^{T}\left(\widehat{\mathbf{R}} - \mathbf{C}_{\mathrm{N}}\right)\left(\mathbf{A}_{\mathrm{S}}^{T}\right)^{-1}\mathbf{A}_{\mathrm{D}}^{T} vec\,\widehat{\mathbf{R}}_n. \tag{23}$$

Similarly to (19), the log-GLRT in (23) can be also understood as a two-step procedure. First, the binary-PPM mixed data is separated from the synchronous autocorrelation matrix $\mathbf{R}$ by using the inverse of the mixture matrix $\mathbf{A}_{\mathrm{S}}$. Second, the hypothesis testing template is built with the separation matrix $\mathbf{A}_{\mathrm{D}}$ and the result is correlated with the data from the n-th symbol synchronous autocorrelation matrix $\widehat{\mathbf{R}}_n$. Note that both $\mathbf{A}_{\mathrm{S}}$ and $\mathbf{A}_{\mathrm{D}}$ are a-priori known at the receiver since they only depend on the time-shift N_{Δ}. Thus, the matrix product $\left(\mathbf{A}_{\mathrm{S}}^{T}\right)^{-1}\mathbf{A}_{\mathrm{D}}^{T}$ can be calculated offline.

B. Divergence maximizing rank-1 approach

The major drawback of the full-rank approach in (23) is that a relatively high computational burden is involved. Note that the $(N_{sf} \times N_{sf})$ matrix $\widehat{\mathbf{R}}_n$ is required and the number of samples per frame N_{sf} may be a large number because of the extremely fine time resolution of UWB signals. In order to reduce complexity, a practical alternative is to adopt a rank-one approach. The problem can be stated as that of finding the best deterministic receiver filter for the incoming random signal. Rank-one approaches for UWB signals have been previously addressed in the literature, for instance, in [33]. However, very specific constraints were imposed such as assuming the modulation format to be orthogonal PPM and forcing the optimal receiver to maximize the signal-to-noise ratio at the receiver output.

In this paper, the difference with previous rank-one approaches is that the proposed criterion does not restrict the PPM modulation to be orthogonal. Thus the maximum delay spread of the end-to-end channel response is allowed to be larger than the PPM pulse spacing N_{Δ}, but smaller than the frame duration in order to avoid interframe interference. In addition, the symmetric Jeffreys divergence between the hypotheses $\mathcal{H}_{+}$ and $\mathcal{H}_{-}$ is adopted here as a reference criterion for minimizing the bit error rate. The Jeffreys divergence or *J-divergence* is a symmetric measure of the difficulty in discriminating between two hypotheses [35]. Therefore a low-rank detector can be optimally designed by selecting those eigen-dimensions from $\mathbf{C}_{\mathbf{g}}$ that maximize the J-divergence.

Similarly to [36], let us denote the J-divergence by $J \doteq \mathrm{E}_{\mathcal{H}_{+}}\left[L(\mathbf{r}_n)\right] - \mathrm{E}_{\mathcal{H}_{-}}\left[L(\mathbf{r}_n)\right]$. Then the

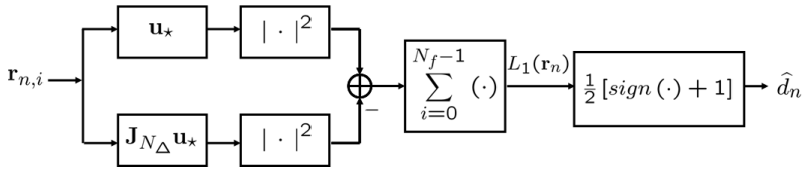

Fig. 2. Optimal rank-one detector for random binary-PPM signals with correlated scattering.

substitution with the log-GLRT test in (10) results in

$$J = Tr\left(\left[\mathbf{C}_+ - \mathbf{C}_-\right]\left[\mathrm{E}_{\mathcal{H}_+}\left[\widehat{\mathbf{R}}_n\right] - \mathrm{E}_{\mathcal{H}_-}\left[\widehat{\mathbf{R}}_n\right]\right]\right) \quad (24)$$

$$= Tr\left(\left[\mathbf{C}_+ - \mathbf{C}_-\right]\left[\mathbf{C}_+ + \mathbf{C}_{\mathrm{N}} - (\mathbf{C}_- + \mathbf{C}_{\mathrm{N}})\right]\right) \quad (25)$$

$$= \|\mathbf{C}_+ - \mathbf{C}_-\|_F^2. \quad (26)$$

The result in (26) indicates that the difficulty in discriminating between $\mathcal{H}_+$ and $\mathcal{H}_-$ is given by the *distance* between the corresponding signal covariance matrices $\{\mathbf{C}_+, \mathbf{C}_-\}$. This is a very important result since it can be used to evaluate the impact of the pulse-spacing N_Δ in the discrimination between $\mathcal{H}_+$ and $\mathcal{H}_-$. An example is shown in Fig. 3 for different channel models of the IEEE 802.15.3a/4 standards.

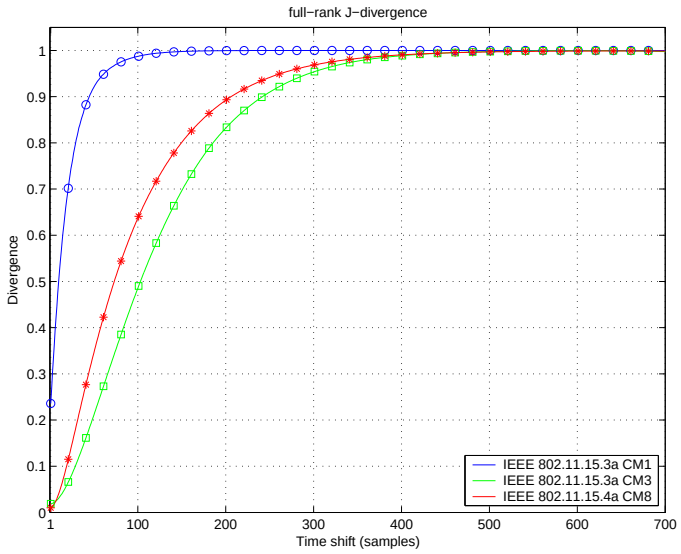

Fig. 3. Normalized J-divergence as a function of the PPM time-shift N_Δ for different channel models. Sampling time 250 ps.

The rank-one approach aims to provide the best deterministic filter that maximizes the J-divergence in (26). To this end, let us express the signal covariance matrix under $\mathcal{H}_+$ as $\mathbf{C}_+ = \mathbf{U}\mathbf{D}\mathbf{U}^T$, with the

($N_{sf} \times N_{sf}$) matrix $\mathbf{U} = \left[\mathbf{u}_0, \mathbf{u}_1, \ldots, \mathbf{u}_{N_{sf}-1}\right]$ containing the eigenvectors of $\mathbf{C}_+$ and the diagonal matrix $\mathbf{D} = diag\left(\lambda_0, \lambda_1, \ldots, \lambda_{Nsf-1}\right)$ containing the corresponding eigenvalues. In this way the log-GLRT in (10) and the J-divergence in (26) can be equivalently expressed as,

$$L_d(\mathbf{r}_n|\mathbf{C_g}) = \sum_{m=0}^{d-1}\sum_{i=0}^{N_f-1} \lambda_m \left[\|\mathbf{u}_m^T\mathbf{r}_{n,i}\|^2 - \|\mathbf{u}_m^T\mathbf{J}_{N_\Delta}^T\mathbf{r}_{n,i}\|^2\right] \tag{27}$$

$$J_d = 2\sum_{p=0}^{d-1}\sum_{q=0}^{d-1}\lambda_p\lambda_q\left[1 - \left(\mathbf{u}_p^T\mathbf{J}_{N_\Delta}\mathbf{u}_q\right)^2\right] \tag{28}$$

with d the dimension of the signal subspace, i.e., the number of significant eigenvalues. For the case of $d = 1$, the rank-one test statistics particularize to

$$L_1\left(\mathbf{r}_n|\mathbf{C_g}\right) = \sum_{i=0}^{N_f-1}\lambda_\star\left(\|\mathbf{u}_\star^T\mathbf{r}_{n,i}\|^2 - \|\mathbf{u}_\star^T\mathbf{J}_{N_\Delta}^T\mathbf{r}_{n,i}\|^2\right), \tag{29}$$

$$\lambda_\star = \frac{\mathbf{u}_\star^H\mathbf{C}_+\mathbf{u}_\star}{\mathbf{u}_\star^H\mathbf{u}_\star}, \tag{30}$$

$$\mathbf{u}_\star = \arg\max_{\mathbf{u}_m} J_1(\mathbf{u}_m) \tag{31}$$

where $\mathbf{u}_\star$ is the optimal receiver filter that maximizes the rank-one J-divergence

$$J_1(\mathbf{u}_m) = 2\lambda_m^2\left[1 - \left(\mathbf{u}_m^T\mathbf{J}_{N_\Delta}\mathbf{u}_m\right)^2\right]. \tag{32}$$

The rank-one J-divergence cost function in (32) is very insightful. Firstly, the structure of the cost function resembles the well-known constant modulus algorithm (CMA) [37], [38]. Secondly, for each of the eigenvectors $\mathbf{u}_m$ of $\mathbf{C}_+$, both the energy contribution for $\mathcal{H}_+$ and the blocking capability for $\mathcal{H}_-$ are evaluated. This is done by the terms λ_m^2 and $\rho_m(N_\Delta) \doteq \mathbf{u}_m^T\mathbf{J}_{N_\Delta}\mathbf{u}_m$, respectively. Thus, the selection criterion for the optimal receiver filter is not only the energy it can extract from the incoming random signal but also the autocorrelation properties it has to block the random signals belonging to the opposite hypothesis.

C. Iterative solution for the divergence maximizing receiver filter

In this section an iterative procedure is proposed to circumvent the computationally demanding task of the complete eigendecompositon of $\mathbf{C_g}$. Apart from the computational savings, the iterative approach provides a more flexible design criterion where transitions between different propagation scenarios can be optimally tracked. This can be done by properly updating the estimated synchronous autocorrelation matrix $\widehat{\mathbf{R}}$ and feeding this information to the iterative criterion.

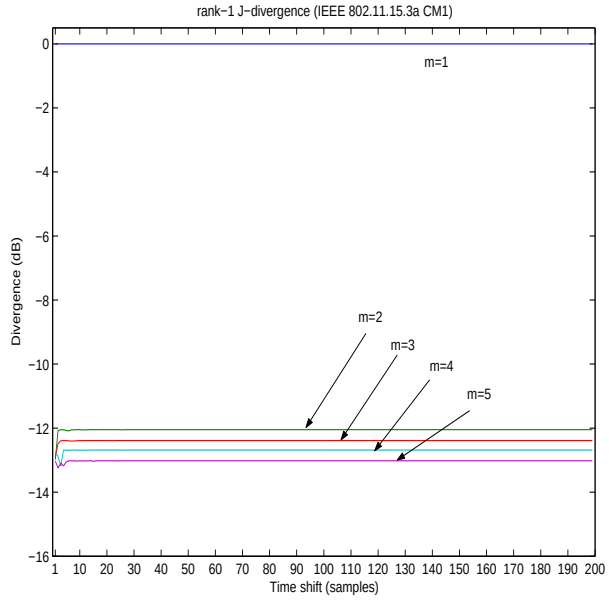

Fig. 4. Evolution of the rank-one J-divergence measure as a function of the PPM time-shift N_Δ for the IEEE802.15.3a channel model CM1 (line-of-sight).

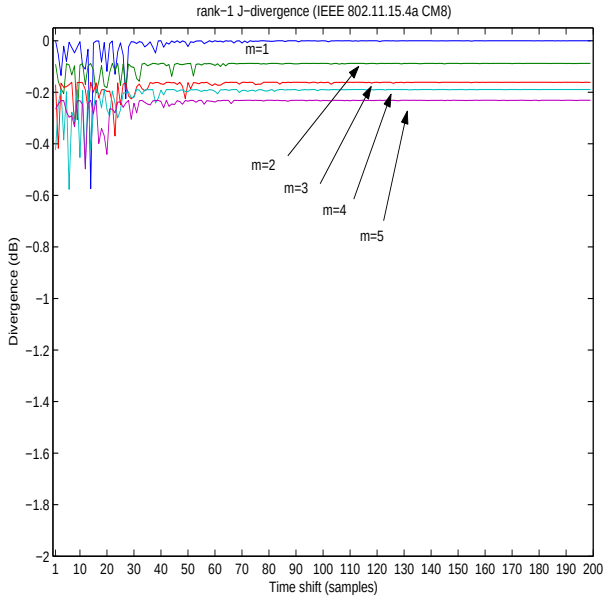

Fig. 5. Evolution of the rank-one J-divergence measure as a function of the PPM time-shift N_Δ for the IEEE802.15.4a channel model CM8 (industrial non line-of-sight)

In the sequel the stochastic gradient descent method is adopted for addressing the iterative optimization in (31)-(32). The recursion is given by

$$\mathbf{u}_\star^{(k+1)} = \mathbf{u}_\star^{(k)} + \mu \left[\nabla_{\mathbf{u}_m} \log J_1(\mathbf{u}_m)\right]\Big|_{\mathbf{u}_m=\mathbf{u}_\star^{(k)}} \tag{33}$$

$$\nabla_{\mathbf{u}_m} \log J_1(\mathbf{u}_m) = \Big[\left(1-\rho_m^2(N_\Delta)\right)\left(\mathbf{C}_+ - \lambda_m \mathbf{I}\right) - \lambda_m \left(\mathbf{u}_m^T \mathbf{u}_m\right) \rho_m(N_\Delta) \mathbf{J}_{N_\Delta}\Big]\mathbf{u}_m. \tag{34}$$

with μ a fixed step size. Note that the gradient descent method in (33) is applied to the logarithm of the rank-one divergence cost function. By doing so, the optimal solution remains the same but the expression for the gradient is simpler. Finally the gradient in (34) is evaluated assuming that the eigenvalue λ_m and the autocorrelation $\rho_m(N_\Delta)$ are defined as

$$\lambda_m \doteq \frac{\mathbf{u}_m^T \mathbf{C}_+ \mathbf{u}_m}{\mathbf{u}_m^T \mathbf{u}_m} \tag{35}$$

$$\rho_m(N_\Delta) \doteq \mathbf{u}_m^T \mathbf{J}_{N_\Delta} \mathbf{u}_m. \tag{36}$$

In practice, an estimate for $\mathbf{C}_+$ can be obtained in a straightforward manner by properly zero-padding the estimate $\widehat{\mathbf{C}}_\mathbf{g}$ proposed in (8). An example of the resulting waveform for the best deterministic rank-one receiver filter is shown in Fig. 6 for the case of the IEEE 802.15.4 CM8 channel model with a sampling time of $T_s = 0.25$ ns, a PPM time-shift of $N_\Delta = 100$ samples and a frame-interval of $N_{sf} = 1000$

samples. This figure shows the exact optimal rank-one receiver filter and the one obtained by using the gradient descent method in (33)-(34). The resulting value of the rank-one J-divergence is also depicted as a function of the number of iterations.

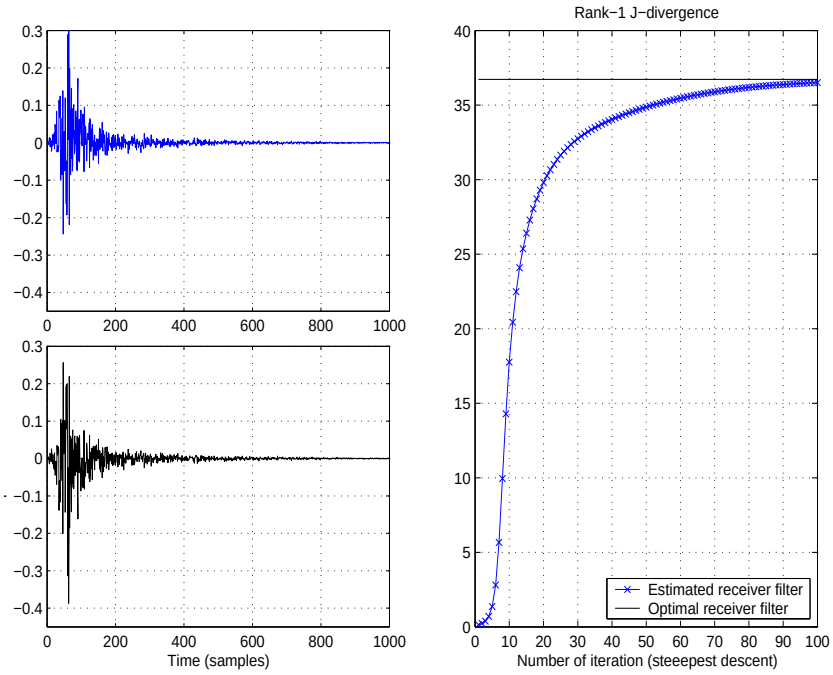

Fig. 6. Best deterministic receiver filter for the IEEE 802.15.4 CM8 channel model according to the proposed iterative optimization of the rank-one J-divergence criterion.

It is important to remark that the proposed iterative approach resembles the well-known Rayleigh quotient iteration (RQI) which provides the maximum eigenvalue and the corresponding eigenvector of any symmetric matrix [39]. The resemblance with the RQI is clear when orthogonal PPM is considered. In that case we have $\rho_m(n) = 0$ for all m when $n \geq N_\Delta$ as a result of the orthogonal transmission. Thus the gradient in (34) simplifies to

$$\nabla_{\mathbf{u}_m} \log J_1(\mathbf{u}_m)\Big|_{\text{orthogonal } 2-\text{PPM}} = [\mathbf{C}_+ - \lambda_m \mathbf{I}]\, \mathbf{u}_m \tag{37}$$

which coincides with the gradient of the RQI [39]. Therefore, the best deterministic receiver filter for orthogonal PPM corresponds to the well-known result of being the maximum eigenvector of $\mathbf{C_g}$ (i.e. $\mathbf{C}_+$). This solution is also found to provide the maximum signal-to-noise ratio at the receiver output. For non-orthogonal PPM, however, the solution is not evident and it must be determined based on the maximization of the rank-one J-divergence cost function in (32).

Finally, note that the proposed rank-one receiver in Fig. 2 can be extended to the case where a set of $d_0 > 1$ eigendimensions are considered. In this situation the receiver architecture can be generalized to the rank-d_0 architecture depicted in Fig. 7. The receiver filters $\mathbf{u}_{\star|d}$ in Fig. 7 are obtained in a sequential manner starting from $\mathbf{u}_{\star|d=1}$ according to the iterative procedure proposed in (33). Once $\mathbf{u}_{\star|d=1}$ is obtained the covariance matrix $\mathbf{C}_+$ must be updated as follows, $\mathbf{C}_{+|d} = \mathbf{C}_{+|d-1} - \mathbf{u}_{\star|d-1}\mathbf{u}_{\star|d-1}^T$ and the iterative procedure in (33) must be started again with the new covariance matrix.

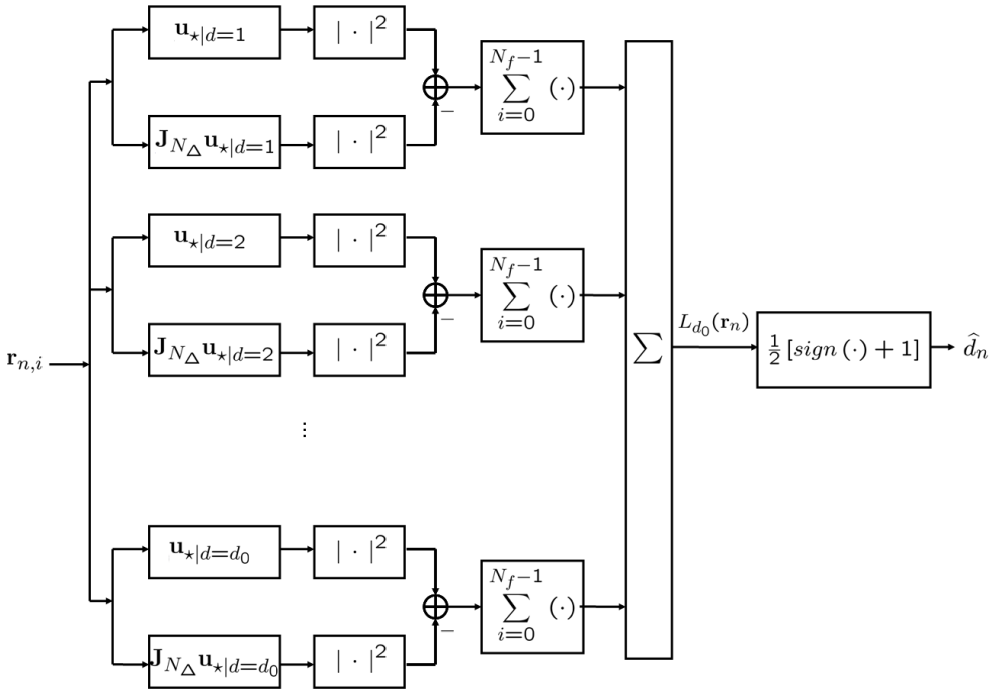

Fig. 7. Extension of the rank-one optimal detector in Fig. 2 to the case $d = d_0$ with $d_0 > 1$.

VII. Simulation Results

In this section, computer simulations are carried out in order to evaluate the performance of the proposed binary-PPM detectors. Two different simulation scenarios are considered:

(A): *Random Gaussian waveforms.* The received waveforms are assumed to be zero-mean random Gaussian processes driven by a given covariance matrix $\mathbf{C_g}$. The processes are non wide-sense stationary with an exponentially decaying power delay profile as in [24]. Two distinctions are made among uncorrelated scattering (US) and correlated scattering (CS) depending on whether the covariance matrix $\mathbf{C_g}$ is diagonal or not.

(B): *IEEE 802.15.3a/4 waveforms.* The received waveforms are generated according to IEEE 802.15.3a and IEEE 802.15.4 channel models.

Regarding the receiver architecture, an all-digital front-end with chip rate sampling is considered. Although it is out of the scope of this manuscript, the adoption of chip-rate sampling may involve a significant complexity from the analog-to-digital conversion (ADC) point of view. In that case, monobit ADCs [40] or channelized ADCs [41] can be considered for a reasonable complexity implementation. It is worth noting that many contributions circumvent this complexity limitation by implementing reduced sampling rates, either at frame-rate or symbol-rate sampling. However, this involves an analog or mixed analog-digital receiver since low sampling rates can only be applied when matched filtering or energy detection has been previously performed in the analog domain.

Similarly to [42], the sampling time is set here to $T_s = 0.125$ ns. The frame duration extends over $N_{sf} = 2000$ samples and a total of $N_f = 20$ frames are conveyed within a symbol duration. The PPM time shift is set to $N_\Delta = 400$ samples unless otherwise specified. Finally, an observation interval of $L = 500$ symbols is used to estimate the synchronous autocorrelation matrix $\mathbf{R}$. With this observation interval, there is no performance degradation by using the estimate $\widehat{\mathbf{R}}$ compared to using the exact $\mathbf{R}$.

The performance results for the proposed receivers are compared with the well-known energy-detector receiver (ED) [31], [32]. The ED receiver is just a simple energy integration. Thus, it can be considered as a simple receiver that assumes the power delay profile to be flat and constant. The fundamentals of an ED receiver are rather simple. For simplicity, let us consider the case $N_f = 1$ with an integration length of N_{ED} samples. Then, the n-th received symbol is decided to be $\widehat{d}_n = 1$ when the energy integrated over the samples from $k = nN_{ss}$ to $k = nN_{ss} + N_{ED} - 1$ is larger than the energy integrated over the samples from $k = nN_{ss} + N_\Delta$ to $k = nN_{ss} + N_\Delta + N_{ED} - 1$. Otherwise, the symbol is decided to be $\widehat{d}_n = 0$. For the results to be presented herein, the $N_{ED} = N_\Delta$. Then, since $N_{sf} > 2N_\Delta$, this strategy for ED can be thought as some kind of noise suppression [43]. Finally, independent frame-to-frame random waveforms are considered except for transmitted-reference (TR) simulations where the waveform remains constant during two frame intervals.

A. Simulation results for random Gaussian waveforms

Experiment 1: Random waveforms with US. In this experiment the received waveforms are modeled as zero-mean Gaussian random processes with uncorrelated samples. The power-delay profile is exponentially decaying with an average delay spread of 100 samples. A total of 1000 waveforms are depicted at the top of Fig. 8 for illustrating the shape of the received waveforms. For this simulation set-up,

two different PPM time-shifts are considered: $N_\Delta = 30$ and $N_\Delta = 400$ samples. Notice that for the case of $N_\Delta = 30$, inter-frame interference (IFI) is being incurred. The receiver performance is analyzed in terms of bit error rate (BER) and it is shown in Fig. 9 as a function of the energy-per-symbol to noise spectral density E_s/N_0. Simulation results are also enclosed for the case of coherent detection with perfect channel state information (CSI) and for the case of transmitted-reference (TR) signaling. In TR schemes, an unmodulated pulse is transmitted prior to each data modulated pulse [44]. In that way the receiver can always take the unmodulated pulse as a reference pulse for correlation, but there is a penalty in power efficiency due to the transmission of unmodulated pulses. This penalty of TR has been compensated in the results of Fig. 9 for a fair comparison of the information detection capability with the rest of the proposed schemes.

From the results in Fig. 9, the full-rank detector based on (23) and the PDP detector based on (19) provide similar performance. Note that the PDP detector just considers the main diagonal of the covariance matrix $\mathbf{C_g}$ whereas the full-rank detector based on (23) estimates the whole covariance matrix $\mathbf{C_g}$. However, the covariance matrix $\mathbf{C_g}$ becomes diagonal in the presence of US and the full-rank detector in (23) becomes the PDP detector. As for the TR detector, the main degradation is caused by the severe noise at the frame-level, making the reference pulse to become a very noisy template. Finally, the poor performance of the rank-one detector is due to the spread of eigendimensions in US. That is, a rank-one contribution is almost negligible due to the large amount of significant eigenvalues of $\mathbf{C_g}$.

Experiment 2: Random waveforms with correlated samples. In this experiment, the received waveforms are modeled as Gaussian random processes with correlated samples. The power delay profile is exponentially decaying with an average delay spread of 100 samples and the temporal lags of the autocorrelation are also set to be exponentially decaying with an average delay spread of 200 samples. A total of 1000 waveforms are depicted at the bottom of Fig. 8 for illustrating the shape of the received waveforms.

The BER performance in terms of the energy-per-symbol to noise spectral density E_s/N_0 is presented in Figure 10. Again, the full-rank detector provides the best performance. The PDP detector degrades because it just considers the main diagonal of $\mathbf{C_g}$ and ignores the rest of the entries, many of them being different from zero when the scattering is correlated. The second best performance for the low-SNR regime is provided by the low-complexity rank-one detector for both $N_\Delta = 30$ and $N_\Delta = 400$ samples. The reason is that the correlatedness of the received waveforms reduces the number of eigendimensions of $\mathbf{C_g}$ compared to the uncorrelated case. As a result, the contribution of a rank-one approximation is now significant compared with the total amount of eigenvalues.

For the case of very small time-shifts N_Δ, the BER performance changes when entering the high-SNR

region. For instance, this can be observed in the left-hand side of Fig. 10 for $E_s/N_0 > 24$ dB. Beyond this E_s/N_0 value, the performance of the rank-one and full-rank detectors experiences a floor effect. This floor effect is a common behavior of most low-SNR estimation and detection techniques when operating in the high-SNR regime, and it can be explained as the noise introduced by the algorithm itself [30]. For the high E_s/N_0 range, the PDP receiver outperforms the full-rank detector because the PDP receiver just considers the main diagonal of $\mathbf{R}$ and thus, self-noise is reduced.

Experiment 3: Random waveforms in the presence of narrowband interferences. In this experiment, the BER performance is evaluated in the presence of interference from IEEE 802.11b WLAN devices. The central frequency for this interference is set to $f_{\mathrm{I}} = 2.4$ GHz with a bandwidth of $\mathrm{BW}_{\mathrm{I}} = 20$ MHz. The simulation parameters are the same as for the previous experiments except for the PPM time-shift that is set here to $N_\Delta = 200$ samples. The signal and noise powers are fixed to result in $E_s/N_0 = 20$ dB. In Fig. 11, the BER performance is evaluated as a function of the interference-to-noise ratio $\frac{P_{\mathrm{I}}}{\sigma_w^2}$. It is interesting to note that, for the case of correlated scattering (right hand side plot in Fig. 11), the rank-one detector becomes the optimal detector when increasing the interference power. This can be seen for $\frac{P_{\mathrm{I}}}{\sigma_w^2} > 6$ dB because the lower bound BER corresponding to the optimal full-rank detector coincides with the BER provided by the low-complexity rank-one detector. Consequently, the rank-one detector turns out to be the optimal detector for interference dominating scenarios. Results are also shown for the LRT in Eq. (9) which is indeed the exact detector. As shown in Fig. 11, a tight match is observed between the exact detector and the proposed full-rank and rank-one detectors in Eq. (10) and Eq. (29). This is especially true for the high-interference region, but a good performance is also obtained for the low-interference region since the low-SNR at the frame-level still remains.

B. Simulation results for the IEEE 802.15.3a/4a channel models

In this section simulation results are provided for the channel models considered in the IEEE 802.15.3a [25] (high data rate) and the IEEE 802.15.4 (low data rate) standards [28]. The simulation set-up is the same as for the case of random waveforms with the exception that only the PPM time-shift of $N_\Delta = 400$ is considered. The selected channel models include both line-of-sight (LOS) and non line-of-sight (NLOS) scenarios. As for LOS scenarios, the channel model CM1 from the IEEE 802.15.3a standard is considered. NLOS scenarios are herein represented by the channel model CM3 from the IEEE 802.15.3a standard and the channel model CM8 from the IEEE 802.15.4a standard. Finally, the channel model for body-area-networks (BAN) within the IEEE 802.15.4 is also considered. The simulation parameters for the BAN channel model assume a distance between transmitter and receiver of 0.1 meters, the floor material

is concrete and the back position of the body.

An important issue to be taken into consideration is the path-dependent propagation of UWB signals. This path-dependent distortion is not considered in the current channel simulation software available from the IEEE 802.15.3a/4 working group. However, and according to the IEEE 802.15.4a final report, the path-dependent distortion can be incorporated by considering the generated taps of the tapped delay line model to be the discrete-time samples of a bandlimited random process (i.e. the random received waveform) [28, p.35]. Therefore, the samples of the received waveforms considered herein are indeed the tap values generated by the standardized software provided by the IEEE working group.

The BER results are presented in Fig. 12 and Fig. 13 for the IEEE 802.15.3a and the IEEE 802.15.4a channel models, respectively. For all the channel models the full-rank detector based on (23) continues to provide the best performance. Moreover, the performance of the PDP receiver based on (19) is found to coincide with the full-rank detector for all the tested channel models except for the CM8. This indicates that the US assumption considered in the PDP detector applies to most of the tested IEEE channel models. Related with this remark, note that the rank-one detector usually provides the worst performance except for the BAN channel. This is due to the fact that the rank-one detector is devoted to propagation environments where the amplitudes of the received samples (not the magnitudes) are correlated and thus, the channel energy is only spread over a small number of eigendimensions. This requirement for the amplitude of the received samples is not fulfilled in most of the considered channel models since we find that the channel energy if spread over a large number of eigendimensions [45]. Thus the performance of the rank-one detector seriously degrades. For a more detailed analysis on the eigenvalue structure of UWB channels, the reader is referred to [45]-[46]. For the BAN channel, however, the reasonable performance of the rank-one detector is in line with the correlated scattering results found in [47].

VIII. Conclusions

A framework for the symbol decision of binary-PPM UWB signals in the absence of inter-frame interference has been presented. The optimal symbol decision statistics are provided and the relationship with previous contributions in the current literature has been revised. Two different analyses for the symbol decision problem have been presented depending on whether the amplitudes of the received waveforms are correlated or not. The correlated scenario is of special interest since it allows a low cost implementation of the optimal symbol detector. To this end, an iterative algorithm is proposed which is based on information-theoretic criteria and allows us to minimize the bit error probability.

APPENDIX A
DERIVATION OF THE LOW-SNR GENERALIZED LIKELIHOOD RATIO TEST

The GLRT provides the optimal decision rule for deciding between the hypothesis $\mathcal{H}_+ : d_n = 1$ and $\mathcal{H}_- : d_n = 0$ based on the probability density function of the received data conditioned on the hypothesis to be tested. According to the channel model in Section II, the conditioned probability density function for the n-th received symbol under $\mathcal{H}_+$ is given by the multivariate Gaussian probability density function,

$$p\left(\mathbf{r}_n|\mathcal{H}_+, \mathbf{C_g}\right) = \prod_{i=0}^{N_f-1} \frac{1}{(2\pi)^{N_{sf}/2}\det^{1/2}\left(\mathbf{C}_+ + \mathbf{C}_{\mathrm{N}}\right)} \exp\left(-\frac{1}{2}\mathbf{r}_{n,i}^T\left(\mathbf{C}_+ + \mathbf{C}_{\mathrm{N}}\right)^{-1}\mathbf{r}_{n,i}\right) \quad \text{(A.38)}$$

with $\mathbf{C}_+ \doteq \mathbf{\Pi C_g \Pi}^T$ the covariance matrix for the signal received under $\mathcal{H}_+$ and $\mathbf{C}_{\mathrm{N}} \doteq \sigma_w^2\mathbf{I} + \mathbf{C}_{\mathrm{I}}$ the covariance matrix for the Gaussian contribution of both the thermal noise and the narrowband interference.

Similarly to (A.38), the conditioned probability density function under the hypothesis $\mathcal{H}_-$ is found by substituting $\mathbf{C}_+$ in (A.38) with $\mathbf{C}_- \doteq \mathbf{J}_{N_\Delta}\mathbf{\Pi C_g \Pi}^T\mathbf{J}_{N_\Delta}$. When both $p(\mathbf{r}_n|\mathcal{H}_+, \mathbf{C_g})$ and $p(\mathbf{r}_n|\mathcal{H}_-, \mathbf{C_g})$ are available, the GLRT results in

$$\Lambda(\mathbf{r}_n|\mathbf{C_g}) = \frac{\det^{1/2}\left(\mathbf{C}_- + \mathbf{C}_{\mathrm{N}}\right)}{\det^{1/2}\left(\mathbf{C}_+ + \mathbf{C}_{\mathrm{N}}\right)} \prod_{i=0}^{N_f-1} \frac{\exp\left(-\frac{1}{2}\mathbf{r}_{n,i}^T\left(\mathbf{C}_+ + \mathbf{C}_{\mathrm{N}}\right)^{-1}\mathbf{r}_{n,i}\right)}{\exp\left(-\frac{1}{2}\mathbf{r}_{n,i}^T\left(\mathbf{C}_- + \mathbf{C}_{\mathrm{N}}\right)^{-1}\mathbf{r}_{n,i}\right)}. \quad \text{(A.39)}$$

The GLRT in (A.39) can be significantly simplified when both the noise and the interference are high-power sources compared with the UWB transmitter. The following assumptions can be done:

***(AS1) Assumption** 1:*

$$\frac{\det\left(\mathbf{C}_- + \mathbf{C}_{\mathrm{N}}\right)}{\det\left(\mathbf{C}_+ + \mathbf{C}_{\mathrm{N}}\right)} \approx 1. \quad \text{(A.40)}$$

Proof: Let us first expand the determinant $\det\left(\mathbf{C}_+ + \mathbf{C}_{\mathrm{N}}\right)$ as follows,

$$\det\left(\mathbf{C}_+ + \mathbf{C}_{\mathrm{N}}\right) = \det\left(\mathbf{C}_+ + \sigma_w^2\mathbf{I} + \mathbf{C}_{\mathrm{I}}\right) = \det\left(\sigma_w^2\left[\sigma_w^{-2}\mathbf{C}_+ + \mathbf{I} + \sigma_w^{-2}\mathbf{C}_{\mathrm{I}}\right]\right) \quad \text{(A.41)}$$

$$= \sigma_w^{2N_{sf}}\det\left(\sigma_w^{-2}\mathbf{C}_+ + \mathbf{I} + \sigma_w^{-2}\mathbf{C}_{\mathrm{I}}\right). \quad \text{(A.42)}$$

Since the noise is considered a high-power source compared to the UWB signal, it is reasonable to assume that $\sigma_w^{-2}\mathbf{C}_+ \approx \mathbf{0}$. Note that the same approximation cannot be applied to the term $\sigma_w^{-2}\mathbf{C}_{\mathrm{I}}$ since both the noise and the interference may have powers on the same order. Consequently, $\det\left(\mathbf{C}_+ + \mathbf{C}_{\mathrm{N}}\right) \approx \sigma_w^{2N_{sf}}\det\left(\mathbf{I} + \sigma_w^{-2}\mathbf{C}_{\mathrm{I}}\right)$. The key point is to notice that this approximation does not depend on the signal covariance matrix $\mathbf{C}_+$. The same conclusion applies when expanding the determinant $\det\left(\mathbf{C}_- + \mathbf{C}_{\mathrm{N}}\right)$, which is also found to be independent of $\mathbf{C}_-$. As a result, it can be stated that $\det\left(\mathbf{C}_+ + \mathbf{C}_{\mathrm{N}}\right) \approx \det\left(\mathbf{C}_- + \mathbf{C}_{\mathrm{N}}\right)$ which confirms the assumption in (A.40). ■

***(AS2) Assumption** 2:*

$$(\mathbf{C}_+ + \mathbf{C}_\mathrm{N})^{-1} \approx \mathbf{C}_\mathrm{N}^{-1} - \mathbf{C}_\mathrm{N}^{-1}\mathbf{C}_+\mathbf{C}_\mathrm{N}^{-1}, \tag{A.43}$$

$$(\mathbf{C}_- + \mathbf{C}_\mathrm{N})^{-1} \approx \mathbf{C}_\mathrm{N}^{-1} - \mathbf{C}_\mathrm{N}^{-1}\mathbf{C}_-\mathbf{C}_\mathrm{N}^{-1}. \tag{A.44}$$

Proof: Let us focus on the proof for (A.43), since the same proof applies also to (A.44) by substituting $\mathbf{C}_+$ with $\mathbf{C}_-$. To proceed, the matrix inversion lemma is considered which states that $(\mathbf{A}+\mathbf{BCD})^{-1} = \mathbf{A}^{-1} - \mathbf{A}^{-1}\mathbf{B}\left(\mathbf{DA}^{-1}\mathbf{B}+\mathbf{C}^{-1}\right)^{-1}\mathbf{DA}^{-1}$, where $\mathbf{A}$ is $(n\times n)$, $\mathbf{B}$ is $(n\times m)$, $\mathbf{C}$ is $(m\times m)$, $\mathbf{D}$ is $(m\times n)$, and the required inverses exist. When applied to (A.43), the inversion lemma results in

$$(\mathbf{C}_+ + \mathbf{C}_\mathrm{N})^{-1} = \mathbf{C}_\mathrm{N}^{-1} + \mathbf{C}_\mathrm{N}^{-1}\mathbf{C}_+\left(\mathbf{C}_\mathrm{N}^{-1}\mathbf{C}_+ + \mathbf{I}\right)^{-1}\mathbf{C}_\mathrm{N}^{-1}. \tag{A.45}$$

Since the noise and the interference sources are considered high-power sources compared to the UWB transmitter, it is reasonable to assume that $\mathbf{C}_\mathrm{N}^{-1}\mathbf{C}_+ + \mathbf{I} \approx \mathbf{I}$ in (A.45). Therefore, the result in (A.45) can be simplified to $(\mathbf{C}_+ + \mathbf{C}_\mathrm{N})^{-1} \approx \mathbf{C}_\mathrm{N}^{-1} + \mathbf{C}_\mathrm{N}^{-1}\mathbf{C}_+\mathbf{C}_\mathrm{N}^{-1}$ which concludes the proof. ■

With the above assumptions the GLRT in (A.39) simplifies to

$$\Lambda(\mathbf{r}_n|\mathbf{C_g}) \approx \prod_{i=0}^{N_f-1} \frac{\exp\left(-\frac{1}{2}\mathbf{r}_{n,i}^T\mathbf{C}_\mathrm{N}^{-1}\mathbf{C}_+\mathbf{C}_\mathrm{N}^{-1}\mathbf{r}_{n,i}\right)}{\exp\left(-\frac{1}{2}\mathbf{r}_{n,i}^T\mathbf{C}_\mathrm{N}^{-1}\mathbf{C}_-\mathbf{C}_\mathrm{N}^{-1}\mathbf{r}_{n,i}\right)}. \tag{A.46}$$

Alternatively, the log-GLRT can be adopted with $L(\mathbf{r}_n|\mathbf{C_g}) \doteq \log\Lambda(\mathbf{r}_n|\mathbf{C_g})$. In this way a more compact expression is obtained as follows,

$$L(\mathbf{r}_n|\mathbf{C_g}) \approx Tr\left(\left[\mathbf{C}_+ - \mathbf{C}_-\right]\mathbf{C}_\mathrm{N}^{-1}\widehat{\mathbf{R}}_n\mathbf{C}_\mathrm{N}^{-1}\right). \tag{A.47}$$

In (A.47), the $(N_{sf}\times N_{sf})$ matrix $\widehat{\mathbf{R}}_n$ stands for the estimate of the synchronous autocorrelation matrix for the n-th received symbol. That is, $\widehat{\mathbf{R}}_n \doteq \frac{1}{N_f}\sum_{i=0}^{N_f-1}\mathbf{r}_{n,i}\mathbf{r}_{n,i}^T$. Finally, two important remarks must be made. First, note that the synchronous autocorrelation matrix $\widehat{\mathbf{R}}_n$ is the sufficient statistics for the symbol decision problem. Second, since the dimensions of $\widehat{\mathbf{R}}_n$ are $(N_{sf}\times N_{sf})$, the symbol decision problem can indeed be addressed on a frame-level basis.

APPENDIX B
IMPACT OF HIGH-POWER NARROWBAND INTERFERENCES

This appendix presents some results on how the interference signals affect the symbol decision statistics. In particular, this involves the evaluation of $\mathbf{C}_\mathrm{N}^{-1}$ in (A.47), with $\mathbf{C}_\mathrm{N}$ the covariance matrix including both the thermal noise and the interference statistics. Let us assume that the frame duration of the UWB signal is small compared with the coherence time of the interference, defined as $T_{ci} \doteq \frac{1}{\mathrm{BW_I}}$. Then the

entries of the interference covariance matrix $\mathbf{C}_{\mathrm{I}}$ in Section II.B can reasonably be approximated by $[\mathbf{C}_{\mathrm{I}}]_{i,j} \approx P_{\mathrm{I}} cos\left(2\pi f_{\mathrm{I}}\left(i-j\right)\right)$. As a result, the whole covariance matrix $\mathbf{C}_{\mathrm{I}}$ can be approximated by $\mathbf{C}_{\mathrm{I}} \approx P_{\mathrm{I}} \mathrm{Re}\left[\mathbf{e}_{f_{\mathrm{I}}}\mathbf{e}_{f_{\mathrm{I}}}^{H}\right] = \frac{P_{\mathrm{I}}}{2}\left[\mathbf{e}_{f_{\mathrm{I}}}\mathbf{e}_{f_{\mathrm{I}}}^{H} + \mathbf{e}_{f_{\mathrm{I}}}^{*}\mathbf{e}_{f_{\mathrm{I}}}^{T}\right]$ with the phasor $\mathbf{e}_{f_{\mathrm{I}}} \doteq \left[1, e^{j2\pi f_{\mathrm{I}}}, \ldots, e^{j2\pi f_{\mathrm{I}}(N_{sf}-1)}\right]^{T}$.

For an asymptotically large observation interval, the covariance matrix $\mathbf{C}_{\mathrm{I}}$ can be expressed in terms of the discrete-time Fourier transform matrix $\mathbf{F}$ as $\mathbf{C}_{\mathrm{I}} \approx \frac{P_{\mathrm{I}}}{2}\mathbf{F}\mathbf{\Lambda}_{f_{\mathrm{I}}}\mathbf{F}^{H}$, where the diagonal matrix $\mathbf{\Lambda}_{f_{\mathrm{I}}}$ has all its entries equal to zero except for the f_{I}-th and the $(1-f_{\mathrm{I}})$-th diagonal entries that are equal to 1. The above expression for $\mathbf{C}_{\mathrm{I}}$ allows us to express the noise plus interference covariance matrix as, $\mathbf{C}_{\mathrm{N}} = \sigma_w^2\mathbf{I} + \mathbf{C}_{\mathrm{I}} \approx \sigma_w^2\mathbf{I} + \frac{P_{\mathrm{I}}}{2}\mathbf{F}\mathbf{\Lambda}_{f_{\mathrm{I}}}\mathbf{F}^{H} = \mathbf{F}\left[\sigma_w^2\mathbf{I} + \frac{P_{\mathrm{I}}}{2}\mathbf{\Lambda}_{f_{\mathrm{I}}}\right]\mathbf{F}^{H}$. Since the covariance matrix $\mathbf{C}_{\mathrm{N}}$ is found to diagonalize with the discrete Fourier transform matrix, the inverse of $\mathbf{C}_{\mathrm{N}}$ can be easily obtained as

$$\mathbf{C}_{\mathrm{N}}^{-1} = \mathbf{F}\left[\sigma_w^2\mathbf{I} + \frac{P_{\mathrm{I}}}{2}\mathbf{\Lambda}_{f_{\mathrm{I}}}\right]^{-1}\mathbf{F}^{H} \approx \sigma_w^{-2}\mathbf{I}. \tag{B.48}$$

The approximation in (B.48) is due to the fact that the number of non-zero entries in $\mathbf{\Lambda}_{f_{\mathrm{I}}}$ is negligible compared with the number of elements in the diagonal of $\mathbf{I}$. Therefore, it is reasonable to assume that $\left[\sigma_w^2\mathbf{I} + \frac{P_{\mathrm{I}}}{2}\mathbf{\Lambda}_{f_{\mathrm{I}}}\right]^{-1} \approx \sigma_w^{-2}\mathbf{I}$. Consequently, the log-GLRT in (A.47) simplifies to

$$L'(\mathbf{r}_n|\mathbf{C}_{\mathbf{g}}) = Tr\left(\left[\mathbf{C}_{+} - \mathbf{C}_{-}\right]\widehat{\mathbf{R}}_n\right) \tag{B.49}$$

where all the irrelevant constant terms have been omitted for the sake of clarity.

REFERENCES

[1] L. Yang and G. B. Giannakis, "Ultra-Wideband Communications: An Idea Whose Time Has Come," *IEEE Signal Processing Mag.*, vol. 21, no. 6, pp. 26–54, November 2004.

[2] *First Report and Order, Revision of Part 15 of the Commission's Rules Regarding Ultra-Wideband Transmission Systems*, April 2002, FCC, Washington, DC. ET Docket 98-153, FCC 02-48.

[3] M. Z. Win, "Spectral Density of Random UWB Signals," *IEEE Commun. Lett.*, vol. 6, no. 12, pp. 526–528, December 2002.

[4] R. W. Ziolkowski, "Properties of Electromagnetic Beams Generated by Ultra-Wide Bandwidth Pulse-Driven Arrays," *IEEE Trans. Antennas Propagat.*, vol. 40, no. 8, pp. 888–905, August 1992.

[5] F. R. Mireles, "On the Performance of Ultra-Wide-Band Signals in Gaussian Noise and Dense Multipath," *IEEE Trans. Veh. Technol.*, vol. 50, no. 1, pp. 244–249, January 2001.

[6] R. C. Qiu, "A Study of the Ultra-Wideband Wireless Propagation Channel and Optimum UWB Receiver Design," *IEEE J. Select. Areas Commun.*, vol. 20, no. 9, pp. 1628–1637, December 2002.

[7] R. C. Qiu, C. Zhou, and Q. Liu, "Physics-Based Pulse Distortion for Ultra-Wideband Signals," *IEEE Trans. Veh. Technol.*, vol. 54, no. 5, pp. 1546–1555, September 2005.

[8] R. J.-M. Cramer, R. A.Scholtz, and M. Z. Win, "Evaluation of an Ultra-Wide-Band Propagation Channel," *IEEE Trans. Antennas Propagat.*, vol. 50, pp. 561–570, May 2002.

[9] U. G. Schuster and H. Bölcskei, "How Different are UWB Channels from Conventional Wideband Channels?" in *Proc. International Workshop on Convergent Technologies*, Oulu, Finland, June 2005.

[10] S. Gezici, H. Kobayashi, H. V. Poor, and A. F. Molisch, "Optimal and Suboptimal Linear Receivers for Time-Hopping Impulse Radio Systems," in *Proc. International Workshop on Ultra Wideband Systems (IWUWBS) Joint with Conference on Ultra Wideband Systems and Technologies (UWBST)*, 18-21 May 2004, pp. 11–15.

[11] X. Chu and R. D. Murch, "The Effect of NBI on UWB Time-Hopping Systems," *IEEE Trans. Wireless Commun.*, vol. 3, no. 5, pp. 1431–1436, September 2004.

[12] M.-K. Oh, B. Jung, R. Harjani, and D. Park, "A New Noncoherent UWB Impulse Radio Receiver," *IEEE Commun. Lett.*, vol. 9, no. 2, pp. 151–153, February 2005.

[13] J. Tang and Z. Xu, "A Novel Modulation Diversity Assisted Ultra-Wideband Communication System," in *Proc. IEEE International Conference on Acoustics, Speech and Signal Processing (ICASSP)*, vol. 3, Philadelphia, USA, March 2005, pp. 309–312.

[14] R. C. Qiu, J. Q. Zhang, and N. Guo, "Detection of Physics-Based Ultra-Wideband Signals Using Generalized RAKE with Multiuser Detection (MUD) and Time-Reversal Mirror," *IEEE J. Select. Areas Commun.*, vol. 24, no. 4, pp. 724–730, April 2006.

[15] R. C. Qiu, C. Zhou, N. Guo, and J. Q. Zhang, "Time Reversal with MISO for Ultrawideband Communications: Experimental Results," *IEEE Antennas Wireless Propagat. Lett.*, vol. 5, pp. 269–273, 2006.

[16] H. L. VanTrees, *Detection, Estimation, and Modulation Theory*. John Wiley and Sons, 2001-2003, vol. I.

[17] S. M. Kay, *Fundamentals of Statistical Signal Processing. Detection Theory*. Prentice Hall, 1998, vol. II.

[18] J. A. López-Salcedo and G. Vázquez, "Waveform-Independent Frame-Timing Acquisition for UWB Signals," *IEEE Trans. Signal Processing*, vol. 55, no. 1, pp. 279–289, January 2007.

[19] C. Carbonelli and U. Mengali, "Synchronization Algorithms for UWB Signals," *IEEE Trans. Commun.*, vol. 54, no. 2, pp. 329–338, February 2006.

[20] Y.-P. Nakache and A. F. Molisch, "Spectral Shape of UWB Signals - Influence of Modulation Format, Multiple Access Scheme and Pulse Shape," in *Proc. 57th IEEE Semiannual Conference on Vehicular Technology (VTC-Spring)*, vol. 4, 22-25 April 2003, pp. 2510–2514.

[21] M. E. Sahin and H. Arslan, "Narrowband Interference Identification Approach for UWB Systems," in *Proc. IEEE Military Communications Conference (MILCOM)*, vol. 3, 17-20 October 2005, pp. 1404–1408.

[22] I. Bergel, E. Fishler, and H. Messer, "Narrow-band Interference Suppression in Time-Hopping Impulse-Radio Systems," in *Proc. IEEE Conference on Ultra Wideband Systems and Technologies*, 2002, pp. 303–308.

[23] A. F. Molisch, "Ultrawideband Propagation Channels-Theory, Measurement and Modeling," *IEEE Trans. Veh. Technol.*, vol. 54, no. 5, pp. 1528–1545, September 2005.

[24] D. Cassioli, M. Z. Win, and A. F. Molisch, "The Ultra-Wide Bandwidth Indoor Channel: From Statistical Model to Simulations," *IEEE J. Select. Areas Commun.*, vol. 20, no. 6, pp. 1247–1257, August 2002.

[25] J. Foerster, *Channel Modeling Sub-Committee Report (Final)*, IEEE P802.15 Working Group for Wireless Personal Area Networks (WPANs), February 2003.

[26] U. G. Schuster and H. Bölcskei, "Ultra-Wideband Channel Modeling on the Basis of Information-Theoretic Criteria," in *Proc. International Symposium on Information Theory (ISIT)*, 4-9 September 2005, pp. 97–101.

[27] J. Karedal, S. Wyne, P. Almers, F. Tufvesson, and A. F. Molisch, "Statistical Analysis of the UWB Channel in an Industrial Environment," in *Proc. IEEE Vehicular Technology Conference (VTC-Fall)*, 2004, pp. 81–85.

[28] A. F. Molisch, *IEEE 802.15.4a Channel Model Final Report*, IEEE P802.15 Working Group for Wireless Personal Area Networks (WPANs), November 2004.

[29] M. Z. Win and R. A. Scholtz, "Ultra-Wide Bandwidth Time-Hopping Spread-Spectrum Impulse Radio for Wireless Multiple-Access Communications," *IEEE Trans. Commun.*, vol. 48, no. 4, pp. 679–691, April 2000.

[30] F. M. Gardner, "Self-Noise in Synchronizers," *IEEE Trans. Commun.*, vol. 28, pp. 1159–1163, August 1980.

[31] A. Rabbachin and I. Oppermann, "Synchronization Analysis for UWB Systems with a Low-Complexity Energy Collection Receiver," in *2004 International Workshop on Ultra Wideband Systems (IWUWBS) Joint with Conference on Ultra Wideband Systems and Technologies (UWBST)*, Kyoto, Japan, May 2004, pp. 288–292.

[32] M. Weisenhorn and W. Hirt, "Robust Noncoherent Receiver Exploiting UWB Channel Properties," in *Proc. International Workshop on Ultra Wideband Systems (IWUWBS) Joint with Conference on Ultra Wideband Systems and Technologies (UWBST)*, Kyoto, Japan, May 2004 2004, pp. 156–160.

[33] Q. T. Zhang and S. H. Song, "UWB Signal Detection Using Eigen-Based Receiver," in *Proc. IEEE International Conference on Communications (ICC)*, vol. 5, 16-20 May 2005, pp. 2867–2871.

[34] M. Weisenhorn and W. Hirt, "ML Receiver for Pulsed UWB Signals and Partial Channel State Information," in *Proc. IEEE International Conference on Ultra-Wideband*, 5-8 September 2005, pp. 180–185.

[35] H. Jeffreys, "An Invariant Form for the Prior Probability in Estimation Problems," in *Proc. Roy. Soc. Lon.*, ser. A, 1946, pp. 453–461.

[36] S. Kullback, *Information Theory and Statistics*. Dover Publications, 1997.

[37] J. R. Treichler and B. G. Agee, "A New Approach to Multipath Correction of Constant Modulus Signals," *IEEE Trans. Acoust., Speech, Signal Processing*, vol. 31, pp. 459–472, April 1983.

[38] A. J. van der Veen and A. Leshem, *Robust Adaptive Beamforming*, J. Li and P. Stoica, Eds. Wiley Interscience, 2005, Chapter 6: Constant Modulus Beamforming.

[39] G. H. Golub and C. F. V. Loan, *Matrix Computations*. Johns Hopkins University Press, 1996.

[40] S. Hoyos, B. Sadler, and G. R. Arce, "Monobit Digital Receivers for Ultrawideband Communications," *IEEE Trans. Wireless Commun.*, vol. 4, no. 4, pp. 1337–1344, July 2005.

[41] W. Namgoong, "A Channelized Digital Ultrawideband Receiver," *IEEE Trans. Wireless Commun.*, vol. 2, no. 3, pp. 502–510, May 2003.

[42] C. Carbonelli and U. Mengali, "M-PPM Noncoherent Receivers for UWB Applications," *IEEE Trans. Wireless Commun.*, vol. 5, no. 8, pp. 2285 – 2294, August 2006.

[43] G. Leus and A. J. V. der Veen, "Noise Suppression in UWB Transmitted Reference Systems," in *Proc. 5th IEEE Workshop on Signal Processing Advances in Wireless Communications (SPAWC)*, 11-14 July 2004, pp. 155–159.

[44] R. T. Hoctor and H. W. Tomlinson, *An Overview of Delay-Hopped, Transmitted-Reference RF Communications*, January 2002, G. E. Research and Development Center, Technical Information Series, pp. 1-29.

[45] R. Saadane, A. Menouni, R. Knopp, and D. Aboutajdine, "Empirical Eigenanalysis of Indoor UWB Propagation Channels," in *Proc. IEEE Global Conference on Communications (GLOBECOM)*, December 2004, pp. 3215–3219.

[46] A. Menouni, R. Knopp, and R. Saadane, "Subspace Analysis of Indoor UWB Channels," *EURASIP Journal on Applied Signal Processing*, vol. 3, pp. 287–295, 2005.

[47] A. Fort, J. Ryckaert, C. Desset, P. D. Doncker, P. Wambacq, and L. V. Biesen, "Ultra-Wideband Channel Model for Communications Around the Human Body," *IEEE J. Select. Areas Commun.*, vol. 24, no. 4, pp. 927–933, April 2006.

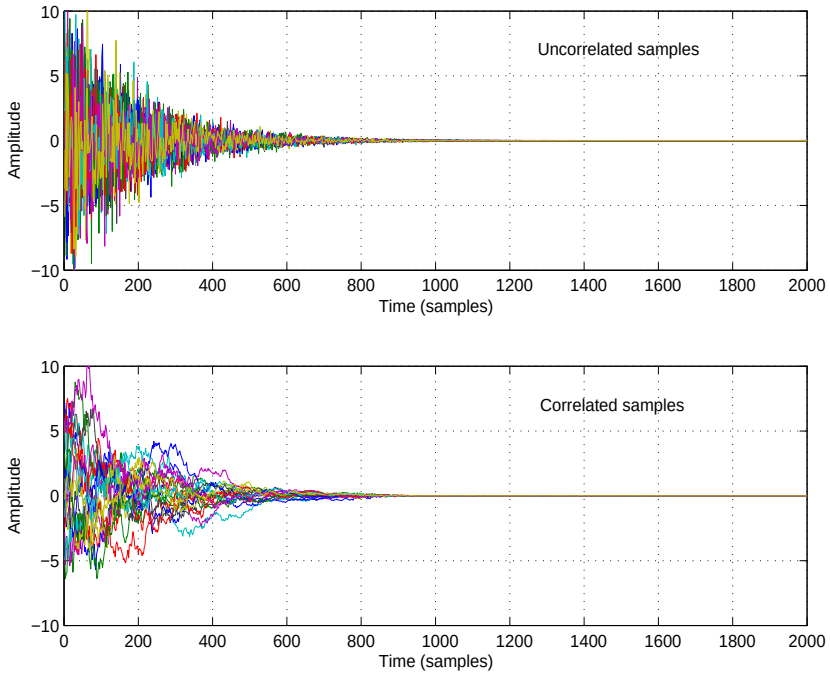

Fig. 8. 1000 realizations of the Gaussian random received waveforms with uncorrelated samples (top) and correlated samples (bottom). The power delay profile is exponentially decaying with average delay spread of 100 samples. For the waveforms with correlated samples, the time-lags of the autocorrelation are also exponentially decaying with an average spread of 200 samples.

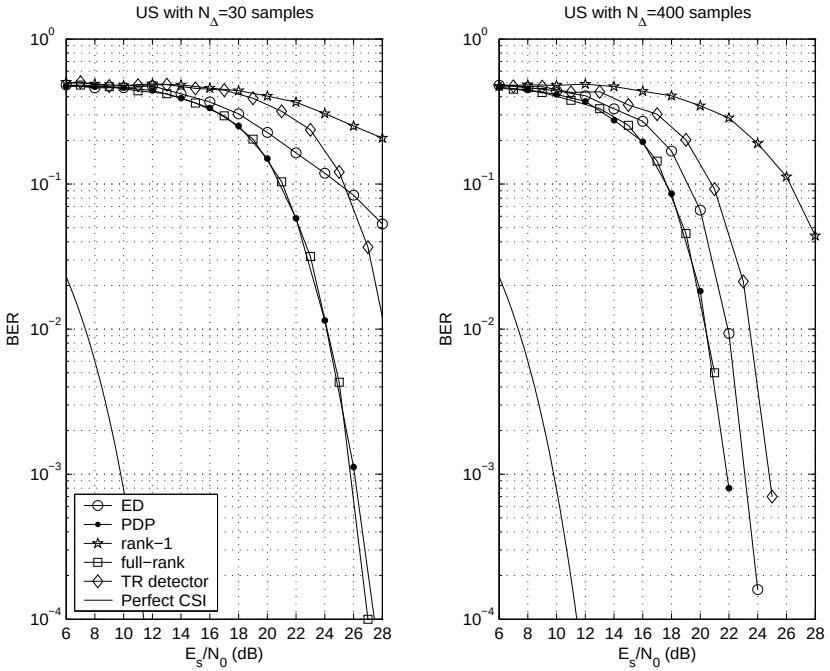

Fig. 9. BER performance for random Gaussian UWB signals with uncorrelated scattering.

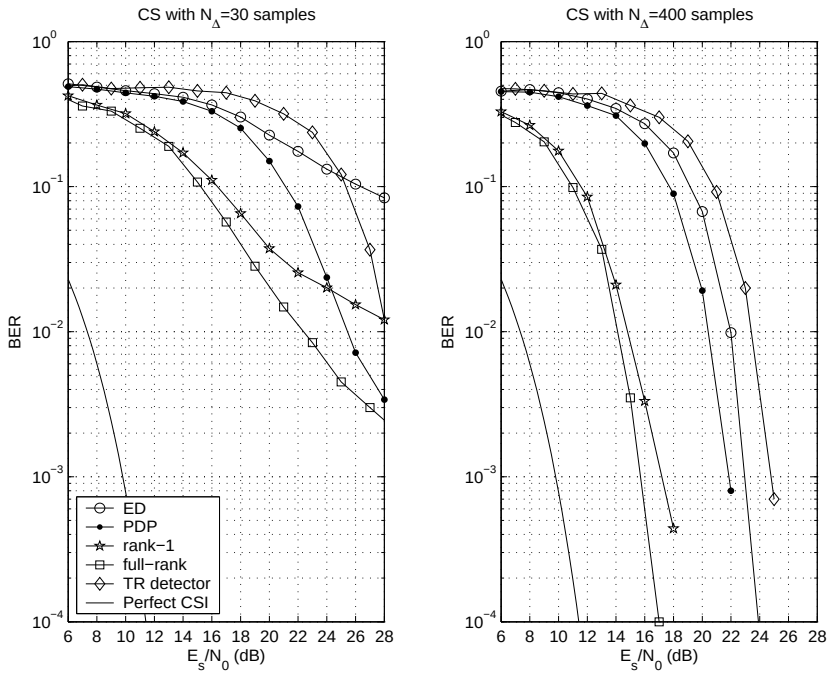

Fig. 10. BER performance for random Gaussian UWB signals with correlated scattering.

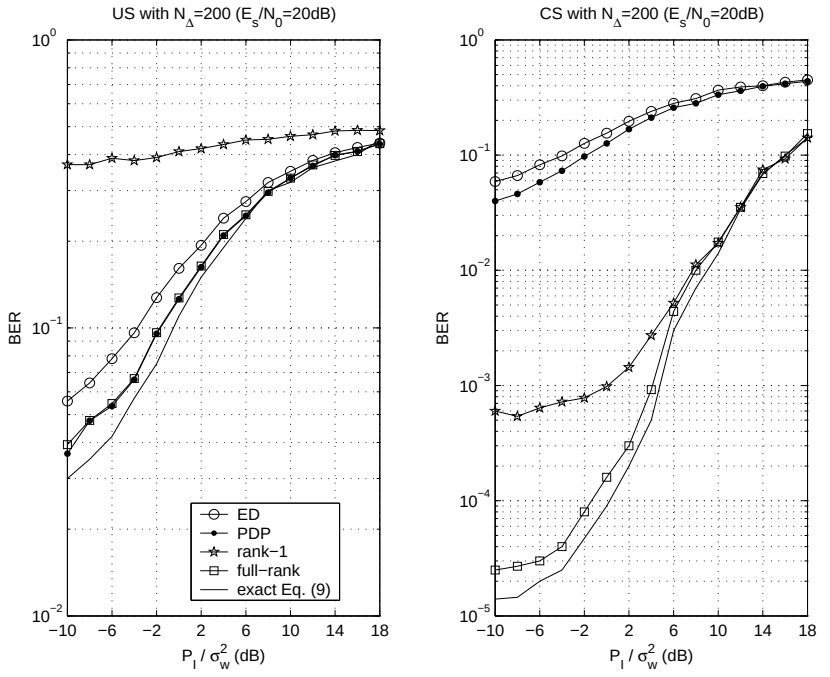

Fig. 11. BER performance for random Gaussian UWB signals in the presence of narrowband interference.

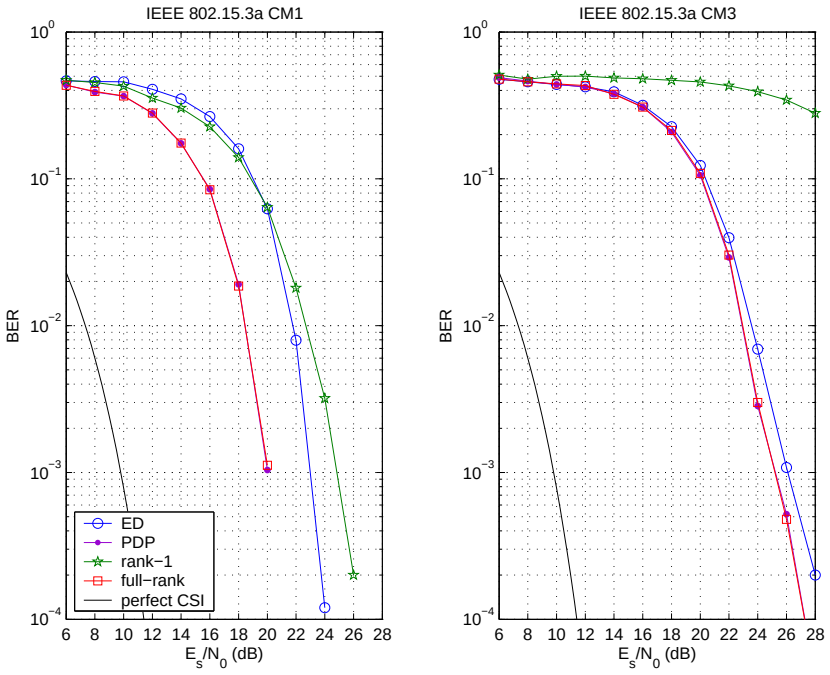

Fig. 12. BER performance for the IEEE 802.15.3a CM1 channel model (line-of-sight) and the IEEE 802.15.3a CM3 channel model (non line-of-sight).

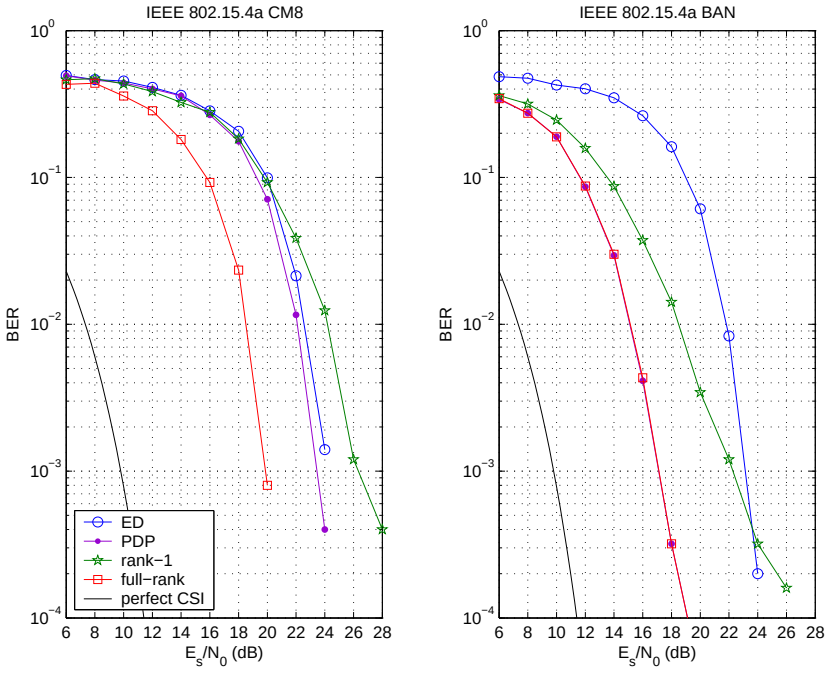

Fig. 13. BER performance for the IEEE 802.15.4 CM8 channel model (industrial non line-of-sight) and the IEEE 802.15.4a BAN channel model (body area network).